CHEMISTRY
A EUROPEAN JOURNAL

DOI: 10.1002/chem.200501195

Self-Assembly of Semifluorinated Dendrons Attached to Electron-Donor Groups Mediates Their π-Stacking via a Helical Pyramidal Column

Virgil Percec,*[a] Martin Glodde,[a] Mihai Peterca,[c] Almut Rapp,[b] Ingo Schnell,[b] Hans W. Spiess,[b] Tushar K. Bera,[a] Yoshiko Miura,[a] Venkatachalapathy S. K. Balagurusamy,[a, c] Emad Aqad,[a] and Paul A. Heiney[c]

Abstract: Semifluorinated first-generation self-assembling dendrons attached via a flexible spacer to electron-donor molecules induce π-stacking of the donors in the center of a supramolecular helical pyramidal column. These helical pyramidal columns self-organize in various columnar liquid crystal phases that mediate self-processing of large single crystal liquid crystal domains of columns and self-repair their intracolumnar structural defects. In addition, all supramolecular columns exhibit a columnar phase at lower temperatures that maintains the helical pyramidal columnar supramolecular structure and displays higher intracolumnar order than that in the liquid crystals phases. The results described here demonstrate the universality of this concept, the power of the fluorous phase or the fluorophobic effect in self-assembly and the unexpected generality of pyramidal liquid crystals.

Keywords: dendrimers · electron-donor groups · liquid crystals · self-assembly

Introduction

Columnar liquid crystals (LC) have received interest as electronic materials after the discovery that hexagonal columnar LCs obtained from discotic molecules exhibit charge carrier mobilities between amorphous polymers and organic single crystals.[1] In addition to high charge carrier mobility, the liquid crystalline state provides a mechanism to process single crystal LC domains of electronic thin films that are not accessible from organic single crystals. By contrast, amorphous and semicrystalline electronically active macromolecules have good processability but display low charge carrier mobility.[2] Although hexagonal columnar LCs obtained from discotic molecules alleviate some of the negative features of polymers and organic single crystals, the engineering of their charge carrier properties requires the synthesis of libraries of complex discotic molecules. Substantial progress has been made on the design and synthesis of electron-donor discotic molecules,[3] and the field has been reviewed.[4] However, there are only limited examples of electron-acceptor discotic molecules.[4c,f,5] Smectic LC phases have been also shown to increase charge carrier mobility of low molecular mass organic[6] and macromolecular[7] compounds. The most recent advance in organic electronic materials was generated by combining the fields of supramolecular chemistry, liquid crystals and molecular electronics to generates the new area of supramolecular electronics.[8]

Columnar LC phases of discotic molecules mediate the arrangement of the aromatic part of the discs in a face-to-face arrangement and thus provide the π–π stacking that is responsible for their increased charge carrier mobility. However, columnar LC can also be self-organized from supramolecular columns that are self-assembled from tapered rather than from discotic molecules.[9] The most notable examples of tapered building blocks are low generation amphiphilic dendrons that can be functionalized with a diversity of groups at their apex.[9] In a recent communication, we have reported preliminary results on a novel strategy to mediate the face-to-face arrangement of both electron-donor and electron-acceptor organic molecules by their attachment to

[a] Prof. V. Percec, Dr. M. Glodde, Dr. T. K. Bera, Dr. Y. Miura, Dr. V. S. K. Balagurusamy, Dr. E. Aqad
Roy & Diana Vagelos Laboratories
Department of Chemistry, University of Pennsylvania
Philadelphia, PA 19104-6323 (USA)
Fax: (+1) 215-573-7888
E-mail: percec@sas.upenn.edu

[b] Dr. A. Rapp, Dr. I. Schnell, Prof. H. W. Spiess
Max Planck Institute for Polymer Research
55021 Mainz (Germany)

[c] M. Peterca, Dr. V. S. K. Balagurusamy, Prof. P. A. Heiney
Department of Physics and Astronomy
University of Pennsylvania
Philadelphia, PA 19104-6396 (USA)

the apex of a self-assembling semifluorinated first-generation dendron or minidendron.[8b] Semifluorination mediates the self-assembly of the first-generation dendrons via the fluorophobic effect[9b,10] and also protects the electronic active core of the supramolecular column against moisture.[8b,f,h] Moreover, co-assembly of these functionalized dendrons between themselves and with complementary amorphous electroactive polymers opens numerous strategies to program various electronic functions of conventional organic and macromolecular materials. This supramolecular electronic system self-repairs its supramolecular structural defects and is self-processable between various electrodes with a desirable arrangement of the supramolecular columns.

In this publication we discuss the scope and limitations of this concept.[8b] The effects of structural modifications of the dendron, spacer and electroactive group from the apex of the dendron on the self-assembly and self-organization processes were examined and will be reported. We will show that our strategy to supramolecular electronic materials mediated by self-assembling dendrons is universal, simple and compatible with a variety of electroactive groups. In addition, the supramolecular columnar structure of the liquid crystal phase reported previously[8b] is maintained with an even higher degree of intracolumnar order in the lower temperature columnar structure that is expected to display even higher charge carrier mobilities than those reported previously.[8b] The electroactive cores used in this study are well known electroactive compounds. They include electron-donors (D) with various shapes that display a wide range of ionization potentials.

Results and Discussion

Synthesis: The structures of the dendrons containing electron-donating groups at their apex that will be discussed in this paper are shown in Figure 1. The synthesis of **(3,4,5)12F8G1-2EONp**, **(3,4,5)12F8G1-BuPy**, **(3,4,5)12F8G1-2EOPy** and **(3,4,5)12F8G1-2EOCz** were reported previously.[8b] These dendrons are derived from the semifluorinated first-generation dendritic acid, **(3,4,5)12F8G1-CO_2H**, containing an alkane or oligoethylene glycol spacer between the acid and the electron-donor groups.

Scheme 1 outlines the synthesis of four new electron-donor groups. 2-[2-(3,5-Dimethoxyphenyl)ethoxy]ethanol (**3**) was synthesized by etherification of the commercially available 3,5-dimethoxyphenol (**1**) with 2-(2-chloroethoxy)-ethanol (**2**) in 57% yield. 3,5-(Dipyrrolidine-1-yl)phenol (**4**) was prepared according to a literature procedure.[11] Alkylation of **4** with 2-(2-chloroethoxy)ethanol (**2**) produced 2-{2-[3,5-(dipyrrolidin-1-yl)phenyl]ethoxy}ethanol (**5**) in 25% yield. The low yield obtained for **5** is due to the instability of compound **4** under the alkylation conditions. Compounds **4** and **5** are sensitive to light and O_2 and should be stored under N_2 in dark. The commercially available phenothiazine (**6**) was sublimed and used immediately for the synthesis of the electron-donating 2-(phenothiazine-10-yl-ethoxy)ethanol (**8**). The latter was prepared in 53% yield according to a modified literature procedure[12] by the alkylation of phenothiazine (**6**) with THP-protected 2-(2-chloroethoxy)ethanol (**7**). In addition to the carbazole linked to diethylene glycol spacer (2EO) reported previously,[8b] the synthesis of a car-

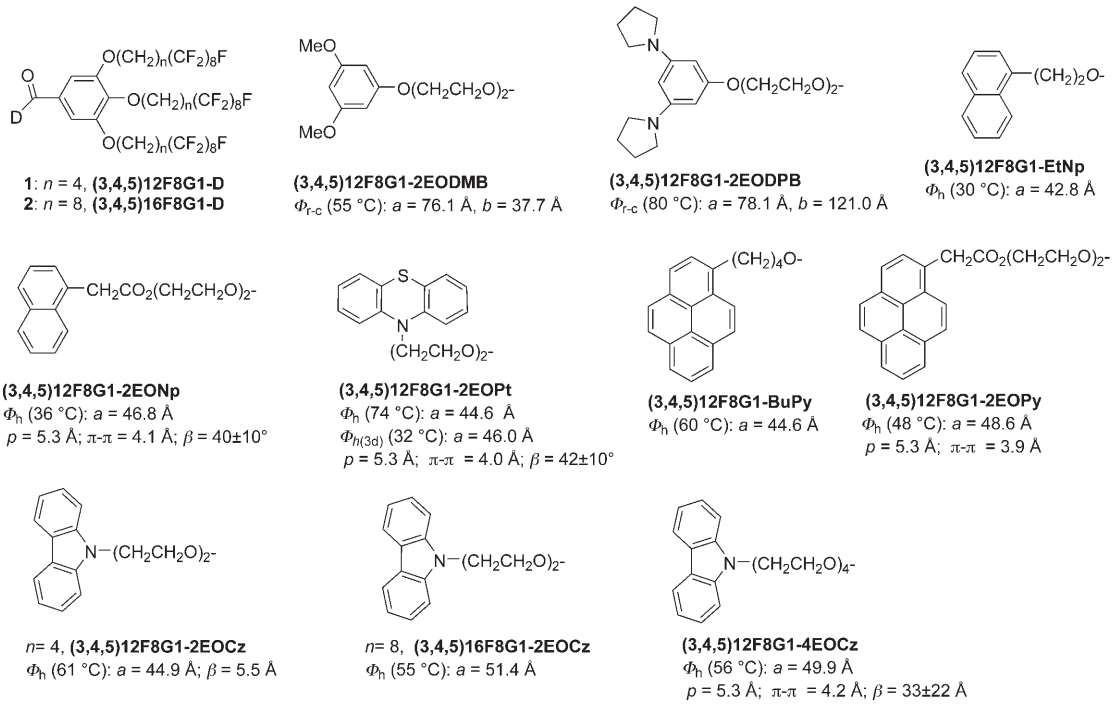

Figure 1. Structures of self-assembling dendrons containing electron-donor groups and the results of the retrostructural analysis of their supramolecular assemblies.

bazole derivative attached to a tetraethylene glycol spacer (4EO) was also achieved. Thus, the N-alkylation of the freshly recrystallized carbazole (**10**) with 2-{2-[2-(2-benzylethoxy)-ethoxy]ethoxy}-*p*-toluene sulfonate (**9**)[13] was best performed by using NaH in DMF at 50 °C. Subsequent Pd/C catalyzed debenzylation afforded compound **11** in 24 % yield.

The synthesis of the new dendrons **(3,4,5)12F8G1-2EODMB** (**D1**), **(3,4,5)12F8G1-2EODPB** (**D2**), **(3,4,5)12F8G1-EtNp** (**D3**), **(3,4,5)12F8G1-2EOPt** (**D5**) and **(3,4,5)12F8G1-4EOCz** (**D10**) was achieved in moderate to high yield by *N*,*N*′-dimethyldicyclohexylcarbodiimide (DCC)/4-dimethylaminopyridinium *p*-toluenesulfonate (DPTS) mediated esterification of the semifluorinated acid **12**[9b,10a] with the hydroxy-terminated electron-donating compounds **3**, **5**, **13**, **8**, and **11**, respectively (Scheme 2). The synthesis of the semifluorinated acid **(3,4,5)16F8-CO$_2$H** (**18**) containing sixteen semifluorinated methylenic groups is shown in Scheme 3. The electroactive dendrons based on **(3,4,5)16F8G1-CO$_2$H** (**18**) are expected to provide higher intracolumnar order than those of the dendrons based on **(3,4,5)12F8G1-CO$_2$H** (**12**) (Scheme 2). The monohydration of 1,7-octadiene (**14**) under hydroboration conditions produced oct-7-ene-1-ol (**15**) in 30 % yield according to a modified literature procedure.[14] The Pd^0-catalyzed addition of perfluorooctyliodide to **15** was performed similar to our previously reported procedure.[13] Reduction with $LiAlH_4$ and subsequent bromination of the corresponding alcohol produced compound **16** in 45 % yield. Etherification of methyl gallate (**17**) with **16** (41 % yield) followed by saponification produced the corresponding acid **(3,4,5)16F8G1-CO$_2$H** (**18**) in 90 % yield. The esterification of carbazole derivative 2-[2-(carbazol-9-yl)-ethoxy]ethanol (**19**)[15] with the semifluorinated acid **18** produced dendron **(3,4,5)16F8G1-2EOCz** (**D9**) in 77 % yield.

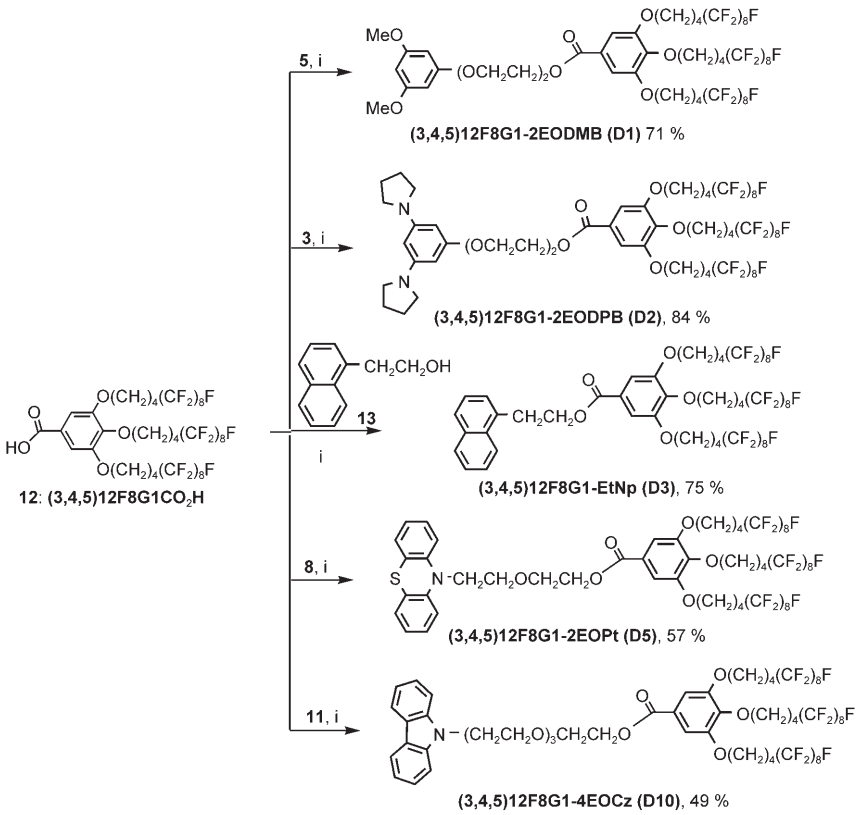

Scheme 2. Dendrimer precursors: i) DCC, DPTS, α,α,α-trifluorotoluene, 55 °C, 12 h.

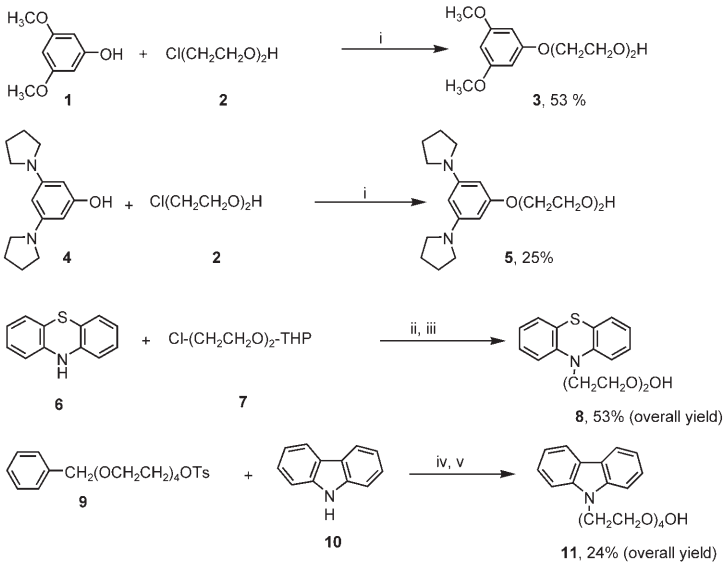

Scheme 1. Synthesis of four new electron-donor groups: i) K_2CO_3, DMF, 70 °C, 12 h; ii) NaH, Bu_2O, 110 °C; iii) HCl_{aq}, MeOH; iv) NaH, DMF, 50 °C, 3 h; v) H_2, Pd/C, EtOH/CH_2Cl_2, 25 °C, 24 h.

Thermal analysis by differential scanning calorimetry (DSC): All dendrons were analyzed by a combination of differential scanning calorimetry (DSC), thermal optical polarized microscopy (TOMP) and X-ray diffraction (XRD) experiments according to methods elaborated previously in our laboratory.[8b,h] The transition temperatures and the corresponding enthalpy changes (kcal mol^{-1}) were determined by DSC with heating and cooling rates of 10 °C min^{-1}. The assignment of various phases was done by a combination of XRD and TOMP according to methods employed in our laboratory.[8b,16] Table 1 summarizes the transition temperatures and the corresponding enthalpy changes for all self-assembling dendrons. All dendrons self-assemble into supra-

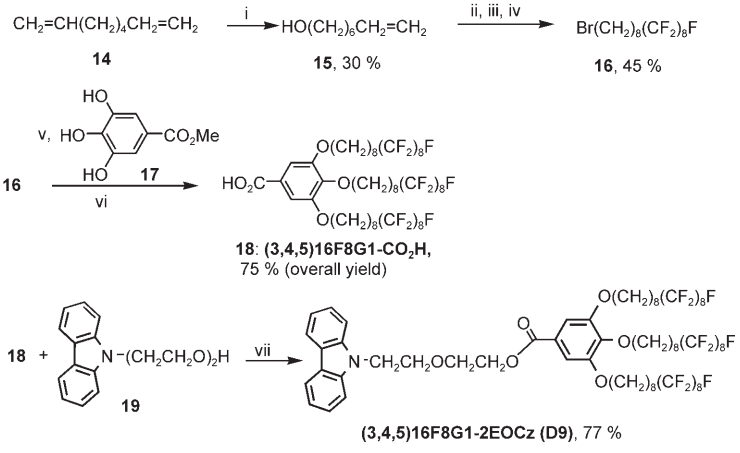

Scheme 3. Synthesis of **18** and **D9**: i) BH_3·THF, then NaOH, H_2O_2; ii) F-$(CF_2)_8$I, [Pd$(PPh_3)_4$], hexanes, Et_2O; iii) $LiAlH_4$, THF then NaOH, H_2O; iv) HBr (48%), aliquate-336; v) K_2CO_3, DMF, 70°C; vi) KOH, EtOH, reflux then HCl_{aq}; vii) DCC, DPTS, α,α,α-trifluorotoluene, 55°C, 12 h.

Table 1. Thermal transitions and corresponding enthalpy changes of the lattices self-organized from supramolecular columns containing electroactive dendrons.

Compound	Thermal transitions [°C] and corresponding enthalpy changes [kcal mol^{-1}][a]	
	Heating	1st Cooling
(3,4,5)12F8G1-2EODMB	Φ^{io}_{r-c} [b],[c] 77.9 (13.32) i[d] Φ^{io}_{r-c} 19 (1.81) Φ^{io}_{r-c} 27 (0.81) Φ_{r-c} 66 (0.48) i	i 62 (0.31) Φ_{r-c} 11 (3.21) Φ^{io}_{r-c}
(3,4,5)12F8G1-2EODPB	Φ^{io}_{r-s} [e] 104 (14.21) i Φ^{io}_{r-s} 15 (1.11) Φ^{io}_{r-s} 49 (−10.22) Φ_h [f] 105 (4.33)	i 50 (0.47) Φ_{r-c} 11 (1.11) Φ^{io}_{r-s}
(3,4,5)12F8G1-EtNp	Φ^{io}_{r-s} 82 (10.03) i Φ^{io}_{r-s} 27 (2.63) Φ^{io}_{r-s} 40 (−4.94) Φ^{io}_{r-s} 82 (9.68) i	i 49 (0.33) Φ_h 19 (2.50) Φ^{io}_{r-c}
(3,4,5)12F8G1-2EONp	Φ^{io}_{r-c} 48 (8.90) Φ_h 75 (0.40) i Φ^{io}_{r-c} 24 (3.07) Φ_h 74 (0.46) i	i 70 (−0.40) Φ_h 16 (3.22) Φ^{io}_{r-c}
(3,4,5)12F8G1-2EOPt	Φ^{io}_{r-s} 61 (8.21) Φ_h 92.0 (0.37) i Φ^{io}_{r-s} 25.4 (1.87)$\Phi^{(io)}_h$ 92 (0.37) i	i 89 (0.39) $\Phi^{(io)g}_h$ 16.0 (1.24) Φ^{io}_{r-s}
(3,4,5)12F8G1-BuPy	Φ^{io}_h 59 (8.20) Φ^{io}_h 63 (−11.00) Φ_h 83 (11.70) i X 13 (1.30) Φ_h 82 (0.67) i	i 78 (0.51) Φ_h 2 X[g]
(3,4,5)12F8G1-2EOPy	Φ^{io}_{r-c} 49 (11.01) Φ_h 97 (0.53) i Φ^{io}_{r-c} −2 k 19 (2.30) Φ_h 97 (0.59) i	i 92 (0.41) Φ_h 7 Φ^{io}_{r-c}
(3,4,5)12F8G1-2EOCz	Φ^{io}_h 39 (2.31) Φ^{io}_h 53 (9.62) Φ_h 75 (1.01) i X 13 k 21 (5.00) Φ_h 75 (0.80) i	i 71 (−0.81) Φ_h 13 (4.91) k 6 X
(3,4,5)16F8G1-2EOCz	Φ^{io}_{r-c} 43 (4.42) Φ_h 63 (0.33) i Φ^{io}_{r-c} 44 (8.54) Φ_h 63 (0.24) i	i 57 (0.32) Φ_h 44 (8.62) Φ^{io}_{r-c}
(3,4,5)12F8G1-4EOCz	X 21 (3.10) Φ_h 81 (0.31) i X 21 (3.10) Φ_h 81 (0.31) i	i 76 (0.51) Φ_h 13 (2.87) X

[a] Data from the first heating and cooling scans are on the first line and data from the second heating are on the second line; [b] Φ_{r-c}, *C2mm* centered rectangular columnar lattice; [c] io: lattice with intracolumnar order; [d] i isotropic; [e] $\Phi_{r-s;}$ *p2mm* simple rectangular columnar lattice; [f] Φ_h, *p6mm* columnar hexagonal lattice; [g] X = unknown phase.

molecular columns that self-organize into various columnar LCs. Hexagonal columnar *p6mm* (Φ_h) LC phases predominate. A centered rectangular columnar *c2mm* (Φ_{r-c}) LC phase was observed in the case of **(3,4,5)12F8G1-2EODMB** and (**3,4,5)12F8G1-2EODPB**. In general, the replacement of the flexible ether spacer by an aliphatic one decreases the temperature range of the columnar LC phase and enhances the tendency towards columnar phases with intracolumnar order or even crystallization. For example, the diethylene glycol spacer in **(3,4,5)12F8G1-2EONp** yields an enantiotropic LC phase, whereas the ethyl spacer **(3,4,5)12F8G1-EtNp** affords only a monotropic phase. Similarly, **(3,4,5)12F8G1-BuPy** (*n*-butyl spacer) exhibits a columnar hexagonal phase with intracolumnar order on first heating, whereas **(3,4,5)12F8G1-2EOPy** (diethylene glycol spacer) shows columnar liquid crystalline phases in all DSC scans. Modification of the core with rigid substituents also reduces the LC temperature range. The dendron **(3,4,5)12F8G1-2EODMB** containing two OCH_3 groups attached to the aromatic core group is enantiotropic after the first heating scan, but **(3,4,5)12F8G1-2EODPB** with two pyrrolidino groups remains only monotropic. Structural modifications of the peripheral design of the semifluorinated dendron reduce the temperature range of the LC phase but increase the melting temperature. Thus, increasing the proportion of methylene groups from $(CH_2)_4$-$(CF_2)_8$F to $(CH_2)_8$-$(CF_2)_8$F decreases the temperature range of the LC phase, as seen by comparing **(3,4,5)12F8G1-2EOCz** enantiotropic LC phase over 60°C) with **(3,4,5)16F8G1-2EOCz** (enantiotropic LC phase over 10°C). Nevertheless, as it will be discussed later, the low temperature phase of **(3,4,5)16F8G1-2EOCz** is generated from supramolecular columns with high degree of intracolumnar order that have the potential to increase the charge carrier mobility above the range of values reported previously.[8b]

Structural and retrostructural analysis by X-ray diffraction: Small-angle (Table 2) and wide-angle X-ray diffraction (XRD) (Table 3) studies on powder and oriented fibers indicate that most of these dendrons form a 2D hexagonal columnar LC phase (Φ_h) at high temperature. This is evidenced by three sharp reflections with the indices (10), (11) and (20). The (10) peak is very strong and the (11) and (20) peaks are weak. The diameters of the supramolecular columns range from 42.8 to 51.4 Å (Table 2). Many dendrons which form a 2D hexagonal columnar phase show an additional, closely related phase at a lower temperature. This corresponds to a weak or moderately strong endotherm in the DSC. In this phase, peaks that were not observed in the 2D hexagonal columnar phase appear. They are slightly broader indicating that there is a fair amount of disorder in the supramolecular columns. The retrostructural analysis of four supramolecular columns by using methods elaborated previously in our laboratory[9d] is summarized in Table 2. The number of dendrons forming a column stratum of 4.7 Å[9d,f,g] varied between 4.1 and 4.6.

Table 2. Structural and retrostructural analysis by XRD of supramolecular columns and their corresponding lattices generated from dendrons containing donor groups.

Compound	Lattice	T [°C]	d Spacings [Å]	a or (a,b) [Å]	ρ_{20}[a] [g cm^{-3}]	μ[b]
(3,4,5)12F8G1-2EODMB	Φ_{r-c}^{io}	0	d_{20} (45.9) d_{11} (40.4) d_{40} (23.2) d_{02} (22.4) d_{22} (20.1)	92.7; 44.7[c]		
	Φ_{r-c}	55	d_{20} (38.1) d_{11} (34.0) d_{02} (18.9) d_{22} (16.7)	76.1; 37.7[c]		
(3,4,5)12F8G1-2EODPB	Φ_{r-s}^{io}	0	d_{10} (40.3) d_{11} (32.1) d_{02} (28.9) d_{20} (20.2) d_{22} (16.2)	39.8; 56.4[d]		
	Φ_{r-c}	80	d_{20} (40.3) d_{13} (36.1) d_{22} (32.2) d_{04} (29.5) d_{06} (20.3) d_{44} (16.4)	78.1; 121.0[c]		
(3,4,5)12F8G1-EtNp	Φ_{r-s}^{io}	20	d_{10} (40.3) d_{01} (33.7) d_{11} (25.7) d_{02} (16.5)	40.6; 32.9[d]		
	Φ_{h}	30	d_{10} (37.0) d_{11} (21.4) d_{20} (18.5)	42.8[e]		
(3,4,5)12F8G1-2EONp	Φ_{r-c}^{io}	15	d_{11} (43.7) d_{20} (39.0) d_{31} (28.9) d_{40} (19.4) d_{13} (16.4)	77.8; 51.4[c]		
	Φ_{h}	36	d_{10} (40.8) d_{11} (20.1) d_{20} (20.1)	46.8[e]	1.49	4.42
(3,4,5)12F8G1-2EOPt	Φ_{r-s}^{io}	10	d_{10} (38.9) d_{01} (32.6) d_{20} (18.9) d_{21} (17.0) d_{12} (15.0)	38.7; 32.8[d]		
	Φ_{h}	74	d_{10} (38.3) d_{11} (22.5) d_{20} (19.5)	44.6[e]		
	Φ_{h}^{io}	32	d_{10} (39.8) d_{11} (22.8) d_{20} (19.8) d_{21} (15.0)	46.0[e]		
(3,4,5)12F8G1-BuPy	Φ_{h}^{io}	24	d_{10} (42.1) d_{20} (21.0)	48.6[e]	1.53	4.12
	Φ_{h}	60	d_{10} (39.0) d_{11} (22.3) d_{20} (19.2)	44.6[e]		
(3,4,5)12F8G1-2EOPy	Φ_{r-c}^{io}	24	d_{11} (44.6) d_{20} (37.9) d_{02} (27.8) d_{31} (22.7) d_{22} (22.1) d_{40} (18.9) d_{13} (17.8)	75.5; 55.07[c]	1.49	4.58
	Φ_{h}	30	d_{10} (42.5) d_{11} (24.2) d_{20} (20.9)	48.6[e]		
(3,4,5)12F8G1-2EOCz	Φ_{h}^{io}	24	d_{10} (41.7) d_{20} (21.1)	48.1[e]	1.62	4.54
	Φ_{h}	61	d_{10} (39.0) d_{11} (22.4) d_{20} (19.5)	44.9[e]		
(3,4,5)16F8G1-2EOCz	Φ_{r-c}^{io}	28	d_{11} (48.3) d_{20} (44.0) d_{02} (28.9) d_{31} (26.3) d_{22} (24.1) d_{40} (22.0) d_{13} (18.7) d_{42} (17.5)	88.2; 57.7[c]		
	Φ_{h}	55	d_{10} (44.6) d_{11} (25.8) d_{20} (22.3)	51.4[e]		
(3,4,5)12F8G1-4EOCz	Φ_{h}	56	d_{10} (43.3) d_{20} (21.6)	49.9[e]		

[a] ρ_{20} = experimental density at 20 °C. [b] Number of monodendrons per 4.7 Å column stratum $\mu = (\sqrt{3}N_A D^2 t_\rho)/2M$(Avogadro's number $N_A = 6.0220455 \times 10^{23}$ mol^{-1}, the average height of the column stratum $t = 4.7$ Å, and M = molecular weight of monodendron. [c] $c2mm$ = centered rectangular (Φ_{r-c}) lattice parameters a and b; $a = hd$, $b = kd$; (h0) and (k0) from diffractions. [d] $p2mm$ = simple rectangular columnar (Φ_{r-s}) lattice parameters a and b; $a = hd$, $b = kd$; (h0) and (k0) from diffractions. [e] $p6mm$ = hexagonal columnar (Φ_h) lattice parameter; $a = 2\langle d_{100}\rangle\sqrt{3}$; $\langle d_{100}\rangle = d_{100} + \sqrt{3}d_{110} + \sqrt{4}d_{200} + \sqrt{7}d_{210})/4$.

Table 3. Structural and retrostructural analysis by wide angle XRD of aligned fibers.

Compound	Phase	T [°C]	Tilt angle [°]	Short-range helical pitch p [Å][a]	π-Stack distance [Å][b]
(3,4,5)12F8G1-2EONp	Φ_h	50	40 ± 10	5.3	4.1
(3,4,5)12F8G1-2EOPt	Φ_h^i	32	20 ± 23	–	3.9
	Φ_h	81	42 ± 10	5.3	4.0
(3,4,5)12F8G1-2EOPy	Φ_h	48	–	5.3	3.9
(3,4,5)12F8G1-2EOCz	Φ_h	65	50 ± 10	5.5	3.9
(3,4,5)16F8G1-2EOCz	Φ_{r-c}^{io}	25	60 ± 8	4.9	3.9
(3,4,5)12F8G1-4EOCz	Φ_h	40	33 ± 22	5.3	4.2

[a] Determined from s_2 in Figure 2. [b] Determined from s_1 in Figure 2.

This noninteger number is expected to induce a helical conformation of the dendrons in the supramolecular column.[8b]

Oriented fibers of these dendrons were studied by small- and wide-angle XRD.[8b] Fibers were extruded from a mini extruder in the LC phase, cooled to room temperature, and then kept in a temperature-controlled oven for recording the XRD patterns at different temperatures. Figure 1 summarizes the analysis of the donor group-containing dendrons. In the well-oriented fibers, sharp reflections with the large maximum in intensity near the equator (perpendicular to the extrusion direction) were observed in the small-angle region in the LC phase. The wide-angle XRD results obtained on oriented fibers are summarized in Table 3. All supramolecular columns consist of pine-tree like or pyramidal helical arrangement of dendrimers.[8b] The tilt angle of the dendrons in these pyramidal supramolecular dendrimers varies between 42 and 22° (Table 3, Figure 2). Their short range helical pitch (s_2 in Figure 2) is between 5.0 and 5.5 Å (Table 3). In agreement with NMR results to be discussed later, this helical pyramidal arrangement of the dendrons mediates the face-to-face arrangement of the electron-donor groups at a distance that varies between 3.9 and 4.2 Å (Table 3). The distance from the s_2 feature in XRD to the equatorial axis (Figure 2 g,h,i) gives the pitch value (p) while the distance from s_2 to the meridional axis gives the radius of rotation of the part of the structure that generates the helical feature. Pitch values larger than 5 Å (Table 3) would be expected to show more than one helical feature. The current data exhibits a single order of diffraction s_2 and therefore, is in agreement with the proposed assignment. The distance between the electron-donor groups determines the charge carrier mobility in the core of the supramolecular columns. These XRD experiments provide only a limited amount of structural information at the molecular level in the supramolecular structure. Therefore, the XRD analysis was complemented by NMR studies carried out in solid state and in solution.

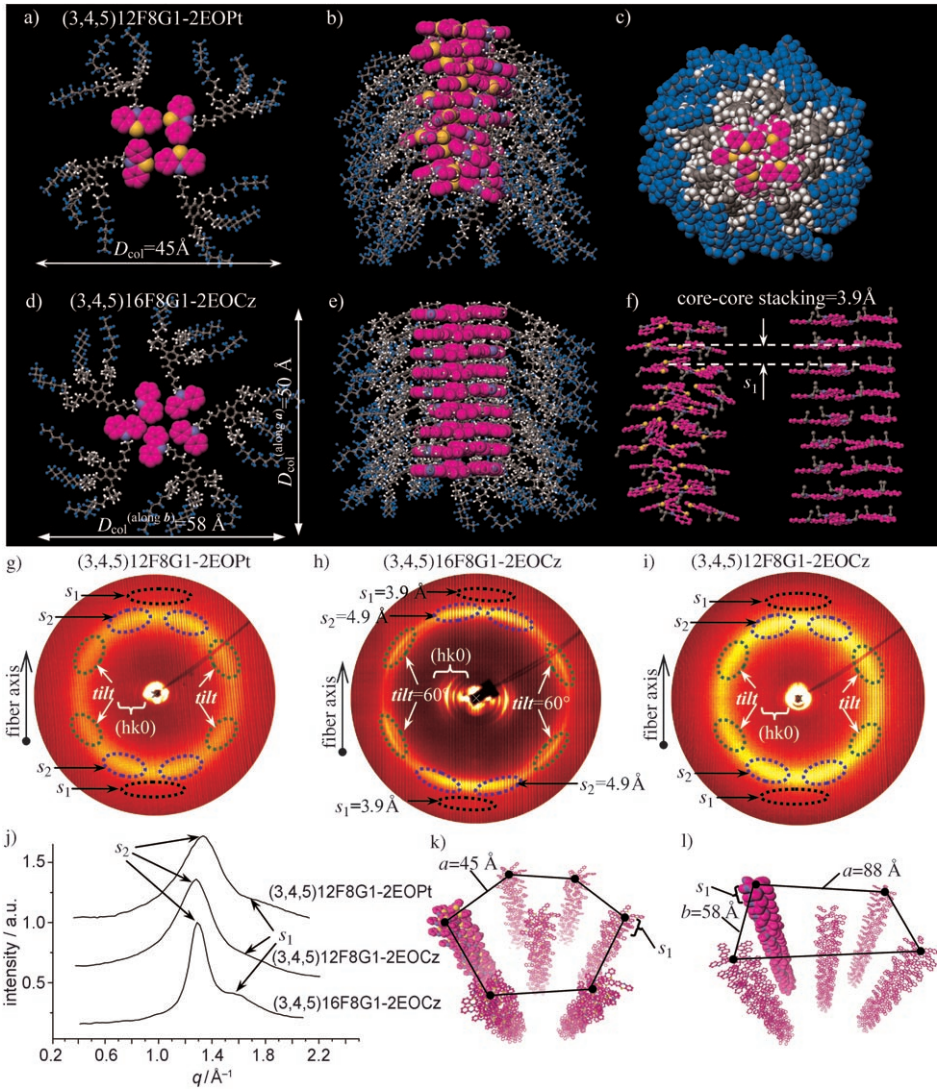

Figure 2. Supramolecular columns self-assembled from **(3,4,5)12F8G1-2EOPt** and **(3,4,5)16F8G1-2EOCz**. a) top-view of one column stratum from **(3,4,5)12F8G1-2EOPt** (**D5**); b) cross-section of the side-view of the column from **(3,4,5)12F8G1-2EOPt**; c) top-view of the column from **(3,4,5)12F8G1-2EOPt**; d) top-view of one column stratum of the column from **(3,4,5)16F8G1-2EOCz**; e) side-view of the cross-section of the column with intracolumnar order from **(3,4,5)16F8G1-2EOCz**; f) details of the **(3,4,5)12F8G1-2EOPt** (left) and **(3,4,5)16F8G1-2EOCz** (right) core-core stacking in the column without (left) and with (right) intracolumnar order; g), h) and i) XRD of the aligned samples of **(3,4,5)12F8G1-2EOPt**, **(3,4,5)16F8G1-2EOCz** and **(3,4,5)12F8G1-2EOCz**; j) stack XRD plot along the meridional region for the **(3,4,5)12F8G1-2EOPt**, **(3,4,5)16F8G1-2EOCz** and **(3,4,5)12F8G1-2EOCz** indicating the position of s_1 and s_2 features; k) and l) schematic of the hexagonal columnar and centered rectangular columnar phases; only the core region is shown. *tilt*-dendron tilt, (hk0) reflections of the hexagonal or rectangular columnar phases, s_1 core–core stacking in agreement with NMR data s_2-dendron helical feature.

Molecular models of the supramolecular pyramidal columns in the LC and higher order phases: Molecular models of the supramolecular helical pyramidal columns were developed based on the XRD results for the Φ_h phase of **(3,4,5)12F8G1-2EOPt** (Figure 2a, b, c, f, g) and for the ordered intracolumnar phase $\Phi^{io}_{r\text{-}c}$ of **(3,4,5)16F8G1-2EOCz** (Figure 2d, e, f, l). The difference between the intracolumnar order in the Φ_h and $\Phi^{io}_{r\text{-}c}$ phase is shown in Figure 2b and e. In Figure 2f the left column belongs to the Φ_h and the right column to the $\Phi^{io}_{r\text{-}c}$ phase. In both cases, the 3.9 Å π–π stacking of the donor groups is observed (see the s_1 feature indicated in Figure 2g, h and j). However, intracolumnar order is much higher in the $\Phi^{io}_{r\text{-}c}$ column of the **(3,4,5)16F8G1-2EOCz** than the Φ_h column of **(3,4,5)12F8G1-2EOCz**. Figure 2j shows that both s_1 and s_2 features are sharper for the **(3,4,5)16F8G1-2EOCz** than the **(3,4,5)12F8G1-2EOPt** or **(3,4,5)12F8G1-2EOCz**. The order along the column increases from approximately four layers, for the **(3,4,5)12F8G1-2EOPt** or **(3,4,5)12F8G1-2EOCz**, to more than 24 layers for **(3,4,5)16F8G1-2EOCz**; the order correlation values were calculated from the full width half maximum of the s_2 feature for the three systems presented in Figure 2j. All low temperature phases from Table 1 maintain the intracolumnar order of their higher temperature liquid crystal phase either in a 2D lattice with intracolumnar order as in the example discussed here or in 3D lattice with intracolumnar order. Therefore, it is expected that even higher charge carrier mobility than the one reported before[8b] must be observed for these phases.

Structural analysis by magic angle spinning NMR spectroscopy: In order to obtain a better understanding of the structure and packing effects, four dendrons **(3,4,5)12F8G1-2EOPy**, **(3,4,5)12F8G1-2EONp**, **(3,4,5)12F8G1-BuPy** and **(3,4,5)12F8G1-EtNp**, were studied by magic angle spinning (MAS) NMR spectroscopy and compared with their non-dendritic precursors 4-pyren-1-yl-butan-1-ol (**PyBuEtOH**) and 2-naphthalen-1-yl-ethanol (**NpEtOH**). Figure 3 shows the proton spectra of these compounds in their solid glassy state, LC phase, in isotropic melt and in $CDCl_3$ solution. The resolution of the spectra increases with temperature from the solid state via the columnar LC phase to the melt. This can be explained by an increase in the mobility of the molecules with temperature, leading to a decrease in the effective dipolar couplings (due to motional averaging) and

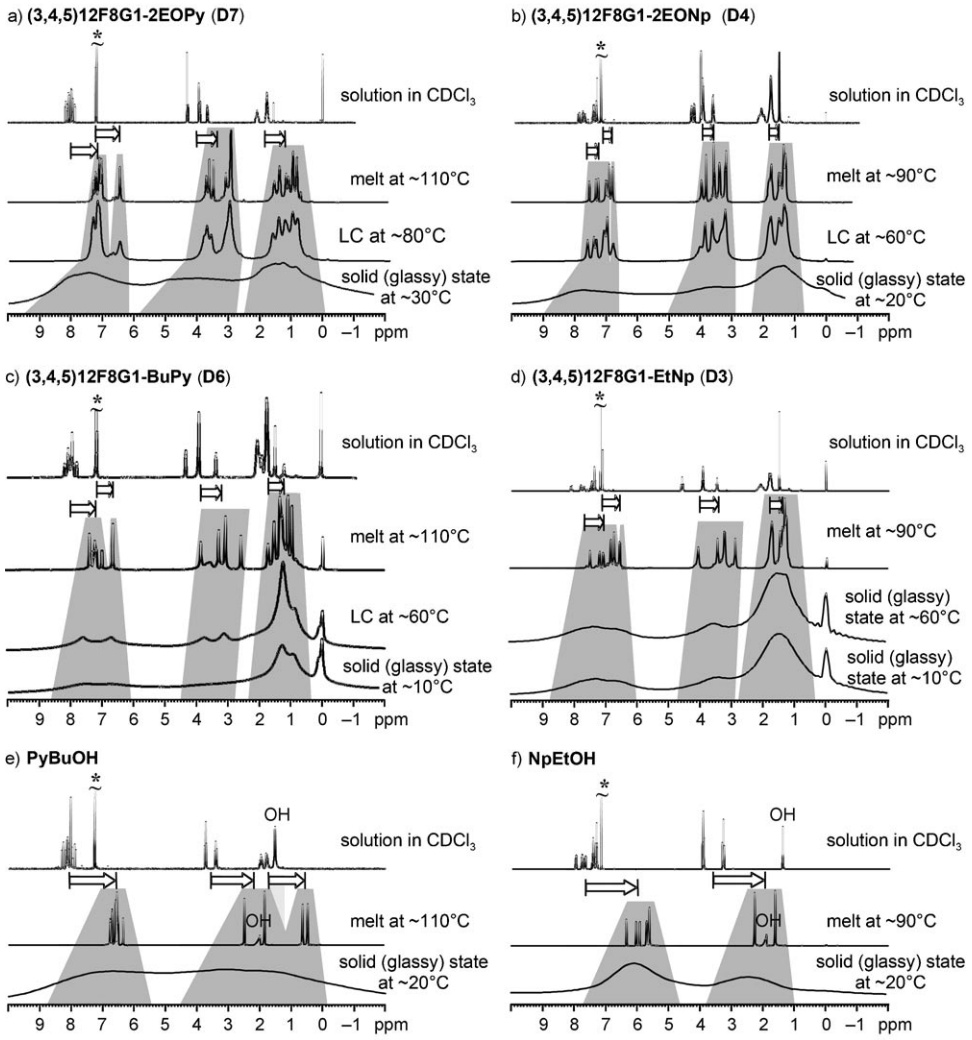

Figure 3. ^{1}H One-pulse spectra of molecules **(3,4,5)12F8G1-2EOPy** (a), **(3,4,5)12F8G1-2EONp** (b), **(3,4,5)12F8G1-BuPy** (c), **(3,4,5)12F8G1-EtNp** (d), PyBuOH (e) and NpEtOH (f) in the intracolumnar ordered solid (glassy) state, the hexagonal columnar LC phase and the melt recorded at 30 kHz MAS. The solution spectra were measured in $CDCl_3$. The white arrows indicate the π-shifts present in the solid-state, the liquid crystalline phase and the melt. The star (*) refers to residual $CHCl_3$ signal.

hence causing less broadening of the resonance lines. Comparing the spectra in the LC phase, much narrower peaks are observed for **(3,4,5)12F8G1-2EOPy** and **(3,4,5)12F8G1-2EONp** than for **(3,4,5)12F8G1-BuPy**. This difference in line width shows that the longer and more flexible ethyleneoxy spacer allows a greater mobility of the molecules in the LC phase as discussed in detail below. Since the LC phase of **(3,4,5)12G1-EtNp**, observed by DSC upon cooling the sample, is rather unstable, it could not be detected by NMR. Figure 3d shows similar proton spectra at 10 and 60 °C upon heating the sample. Thus, the intracolumnar ordered solid or glassy state of **(3,4,5)12G1-EtNp** persists at elevated temperatures as compared to **(3,4,5)12F8G1-BuPy**, which shows a columnar LC phase at 60 °C and hence a significantly narrower linewidth. Table 4 summarizes the chemical shift values of the different CH_n groups and the resultant π-shifts for all six molecules.

By comparison of the solution spectra to the bulk spectra (solid, LC and melt), it becomes apparent that there are π-shifts present to lower frequencies for all resonances (aromatic, OCH_2 and alkyl) in all six molecules, as indicated by the white arrows in Figure 3. Generally, similar π-shifts mean similar π-electron densities surrounding the respective proton in a molecular assembly, pointing at a similar packing of the molecules. Comparing the π-shifts of the aromatic, OCH_2 and alkyl groups in each molecule for the melt, the LC (Φ_h) and the intracolumnar ordered solid phase, two important points are to be noted: i) for **(3,4,5)12F8G1-2EOPy** and **(3,4,5)12F8G1-2EONp**, the π-shifts observed for the aromatic and the OCH_2R protons increase when going from the intracolumnar ordered solid to the LC phase, but remain similar for the transition to the melt. Therefore, the π-electron density of the LC phase and the melt must be comparable, suggesting a similar arrangement of the molecules in both phases. Hence, the columnar structure of the liquid crystalline phase is expected to persist in the melt. The difference in π-shifts observed for the solid and the LC phase can be explained in terms of a slightly different packing of the molecules in the column. In the intracolumnar ordered solid phase, the assembly might be more kinetically controlled, while in the LC phase the thermodynamically preferred arrangement is achieved. ii) For **(3,4,5)12F8G1-BuPy** and **(3,4,5)12F8G1-EtNp** the observed π-shifts are comparable for all phases. Therefore, the π-electron density and, thus, also the molecular assembly in the column are similar in all phases. For a quantitative investigation of the π-shifts, it is necessary to compare the chemical shift of the individual CH_n groups observed in solution with the corresponding chemical shift in the bulk. Therefore, assignment of the different peaks was carried out by 2D Double Quantum (DQ) spectra in addition to the relative intensities of the peaks. Table 4 summarizes the chemical shift values of the different CH_n groups and the resultant π-shifts for all six molecules.

Table 4. ^{1}H NMR Chemical Shifts Observed for the Different CH and CH_2 Groups of **(3,4,5)12F8G1-2EOPy**, **(3,4,5)12F8G1-2EONp**, **(3,4,5)12F8G1-BuPy**, **(3,4,5)12F8G1-EtNp**, **PyBuOH** and **NpEtOH** in solution and in the melt (~100 °C).

	Solution δ(^{1}H) [ppm]	Melt δ(^{1}H) [ppm]	π shift $\Delta\delta$ [ppm]	Solution δ(^{1}H) [ppm]	Melt δ(^{1}H) [ppm]	π shift $\Delta\delta$ [ppm]
	(3,4,5)12F8G1-2EOPy			**(3,4,5)12F8G1-2EONp**		
pyrene/ napthalene	7.8–8.2	6.9–7.4	~0.9	7.2–7.8	6.8–7.5	~0.4
arom CH (dendron)	7.2	6.4	0.8	7.1	6.7	0.4
OCH_2R	3.9	2.9	1.0	3.9	3.1	0.8
OCH_2CH_2 (spacer)	4.2	3.6	0.6	4.2	3.9	0.3
OCH_2CH_2 (spacer)	4.2	3.7	0.5	4.1	3.8	0.3
OCH_2CH_2 (spacer)	3.6	3.0	0.6	3.5	3.3	0.2
Py-/Np-CH_2	4.2	3.4	0.8	3.9	3.5	0.4
	(3,4,5)12F8G1-BuPy			**(3,4,5)12F8G1-EtNp**		
pyrene/ napthalene	7.7–8.2	6.9–7.4	~0.8	7.2–8.1	6.6–7.5	~0.6
arom CH (dendron)	7.2	6.6	0.6	7.0	6.5	0.5
OCH_2R	3.9	3.0, 3.2[a]	0.9, 0.7[a]	3.8	3.1, 3.3[a]	0.7, 0.5[a]
CH_2 (spacer)	4.3	3.8	0.6	4.5	4.0	0.5
Py/Np-CH_2	3.3	2.5	0.8	3.4	2.8	0.6
	PyBuOH			**NpEtOH**		
pyrene/ naphthalene	7.8–8.3	6.3–6.8	1.5	7.2–8.0	6.2–7.0	1.0
CH_2 ("spacer")	3.5	2.1	1.4	3.5	2.5	1.0
CH_2 ("spacer")	1.8	0.5	1.3			

[a] The first and second value correspond to the 3,5 and 4-substituted OCH_2R groups on the aromatic ring, respectively.

The two-dimensional DQ spectra in Figure 4 facilitate the assignment of the different resonances, because they provide information about through-space ^{1}H–^{1}H proximities. If two protons are in close proximity in the material, they will share the same double-quantum frequency, which is the sum of the single quantum frequencies of the two nuclei involved. Therefore, different proton sites that are in close proximity appear as so-called cross peaks in a DQ spectrum. Looking at the spectrum of **(3,4,5)12F8G1-2EOPy**, it is apparent that the diagonal and cross-peaks between δ 6.9 and 7.4 ppm must arise from the pyrene core of the molecule (marked purple in the spectrum), while the resonance at 6.4 ppm belongs to the two aromatic protons of the dendron. As expected, the latter shows a cross-peak to the adjacent OCH_2R groups (2.9 ppm) of the alkyl chains (depicted in dark green) and, in addition, also a weak cross-peak to other groups of the alkyl chains (depicted in light green). The cross-peaks marked in blue at 3.7–3.6 and 3.0 ppm correspond to the resonances of the neighboring groups in the spacer. The orange region in the DQ spectrum (Figure 4) indicates cross-peaks between the OCH_2R and the other CH_2 groups of the alkyl chains. Finally, there is a weak cross-peak observed between the resonances at δ 8.4 and 3.4 ppm (marked pink). Hence, δ 3.4 ppm must be the chemical shift belonging to the pyrene-CH_2 protons, since it is the only one expected to show a proximity to protons of the pyrene ring. Thus, all the resonances observed for the LC phase and the melt in the spectrum in Figure 3a could be assigned, and the result agrees well with the relative intensities of the proton peaks. The peaks of the other three molecules **(3,4,5)12F8G1-2EONp**, **(3,4,5)12F8G1-BuPy** and **(3,4,5)12F8G1-EtNp** have been assigned in an analogous manner. For 4-pyren-1-yl-butan-1-ol (**PyBuOH**) and 2-naphthalen-1-yl-ethanol (**NpEtOH**) the assignment is obvious. The proton chemical shifts in solution and in the melt are summarized in Table 4.

Looking at the π-shifts observed for the polycyclic aromatic protons (pyrene and naphthalene) listed in Table 4, the shifts observed for **(3,4,5)12F8G1-2EOPy** and **(3,4,5)12F8G1-BuPy** ($\Delta\delta = 0.9$ and 0.8 ppm, respectively) are more pronounced than for **(3,4,5)12F8G1-2EONp** and **(3,4,5)12F8G1-EtNp** ($\Delta\delta = 0.4$ and 0.6 ppm, respectively; Table 4). These π-shifts must be an effect of the stacking of the pyrene and naphthalene rings. Therefore, it is not surprising that the pyrene rings, being a larger polycyclic aromatic unit, induce stronger π-shifts than the naphthalene rings. This is also in good agreement with the X-ray diffraction data, since it shows a slightly smaller π–π-stacking distance for **(3,4,5)12F8G1-2EOPy** than for **(3,4,5)12F8G1-2EONp** (Table 3). For the aromatic protons of the dendron, π-shifts similar to those of the polycyclic aromatic protons are observed. Again, they are larger for **(3,4,5)12F8G1-2EOPy** and **(3,4,5)12F8G1-BuPy** ($\Delta\delta$ = 0.8 and 0.6 ppm, respectively) than for **(3,4,5)12F8G1-2EONp** and **(3,4,5)12F8G1-EtNp** ($\Delta\delta$ = 0.4 and 0.5 ppm, respectively). Without taking the possibility of *backfolding* into account, the π-shifts observed for the aromatic protons of the dendron can only be induced by the aromatic rings of neighboring dendrons. A shift of 0.8–0.4 ppm to lower frequencies can be induced by a single aromatic ring located above or below the respective proton, at a distance of 3.5–4.5 Å.[17] This suggests a helical arrangement that supports the XRD results. In this assembly one aromatic proton of the dendron is located underneath the aromatic ring of the adjacent dendron at an average distance of approximately 3.5–4.5 Å (depending on the molecule). The other aromatic proton lies above the aromatic ring of the neighboring dendron on the other side, also at an average distance of approximately 3.5–4.5 Å.

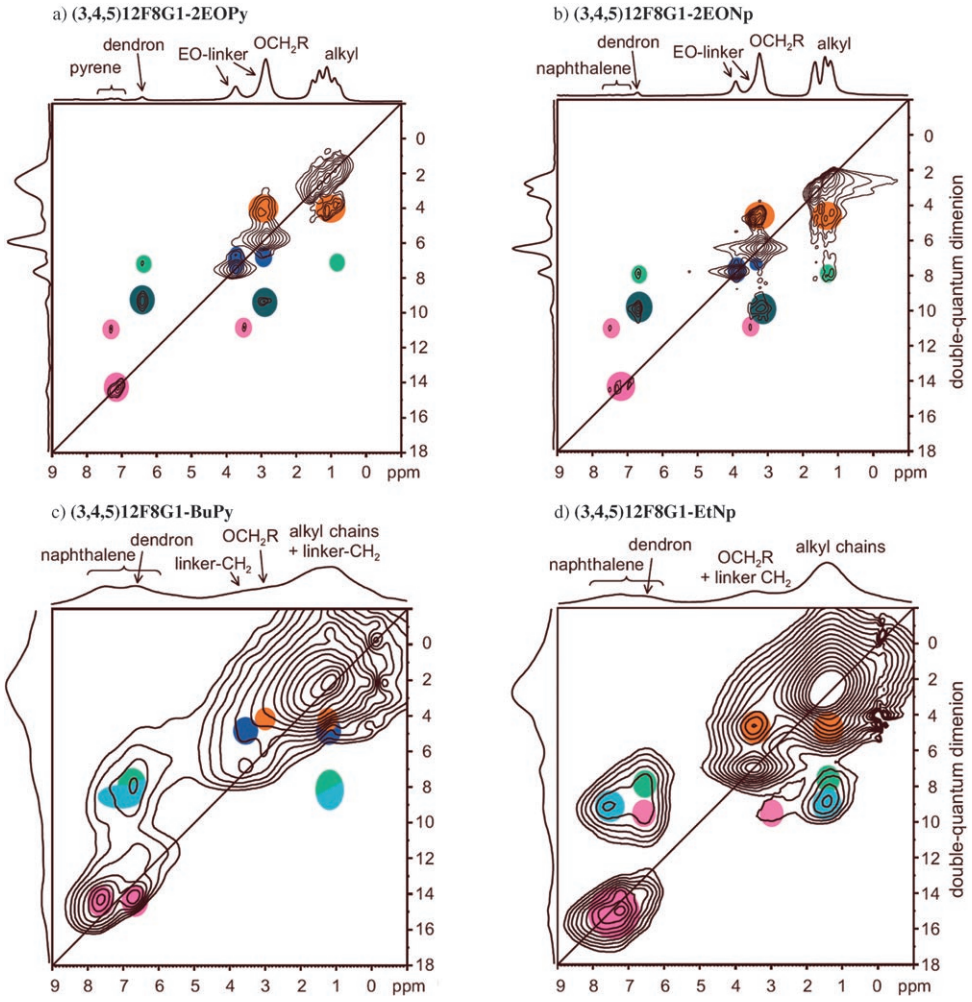

Figure 4. Two-dimensional double-quantum (DQ) spectra of **(3,4,5)12F8G1-2EOPy**, **(3,4,5)12F8G1-2EONp**, **(3,4,5)12F8G1-BuPy** in the LC phase and **(3,4,5)12F8G1-EtNp** in the intracolumnar ordered solid phase since its LC phase is not stable. The spectra were recorded at 60–80 °C, at 30 kHz MAS with an excitation time of four rotor periods ($\tau_{exc}=4\tau_R$) for **(3,4,5)12F8G1-EOPy** and **(3,4,5)12F8G1-2EONp** and two rotor periods ($\tau_{exc}=2\tau_R$) for **(3,4,5)12F8G1-BuPy** and **(3,4,5)12F8G1-EtNp**.

The resonances between δ 2.8 and 4.5 ppm in Figure 4 correspond to the OCH_2R and the spacer protons. Again, larger π-shifts are observed for the two molecules with a pyrene core than for the molecules with a naphthalene core. Comparing the different resonances listed in Table 4, it is apparent that the OCH_2R protons of the alkyl chains experience stronger π-shifts than the spacer protons. Out of the protons of the spacer, the group next to the pyrene or naphthalene ring (Py-/Np-CH_2 in Table 4) experiences the most pronounced π-shifts. This is not surprising, because the pyrene and naphthalene rings are displaced with respect to each other in the column, so that the Py/Np-CH_2 groups are influenced by the shielding effects of the pyrene/naphthalene rings above and below. From a sterical point of view and neglecting backfolding effects, the OCH_2R groups can only experience ring-current effects from dendritic aromatic rings of neighboring molecules, while the groups of the spacer can also be influenced by the π-electrons of the polycyclic aromatic core. Nevertheless, the π-shifts observed for the spacer groups are on average weaker. Therefore, the spacer unit must be spatially separated to a large extent from the polycyclic aromatic core and the dendritic unit, which is discussed in more detail below.

With respect to the OCH_2R groups another interesting feature should be mentioned. The spectra of **(3,4,5)12F8G1-BuPy** and **(3,4,5)12F8G1-EtNp** show two different resonances for the OCH_2R groups in the melt and LC phase, while for **(3,4,5)12F8G1-2EOPy** and **(3,4,5)12F8G1-2EONp** only one resonance is observed. These two resonances can be attributed to different π-shifts experienced by the OCH_2R groups in 3,5- and 4-position on the dendritic aromatic ring that depend on the spacer unit. Short and rigid spacer units, as in **(3,4,5)12F8G1-BuPy** and **(3,4,5)12F8G1-EtNp**, lead to an arrangement of the dendrons in the column where the 3,5- and 4-OCH_2R protons experience different π-shifts from neighboring aromatic rings, while longer and more flexible spacers, as in **(3,4,5)12F8G1-2EOPy** and **(3,4,5)12F8G1-2EONp**, give rise to an arrangement of the dendritic groups where all OCH_2R groups experience the same π-shifts.

Larger π-shifts are also observed for **PyBuOH** ($\Delta\delta=$ 1.5 ppm) as suppose to **NpEtOH** ($\Delta\delta=1.0$ ppm) listed in Table 4. When comparing **PyBuOH** and **NpEtOH** with the respective dendritic molecules, however, significantly larger π-shifts are observed for those precursors. This can be explained in terms of a higher π-electron density that arises from a different not columnar packing of the molecules. Therefore, this demonstrates that the columnar structure is induced primarily by the dendrons and not by the polycyclic aromatic rings.

Separation of aromatic and aliphatic region: A helical-type arrangement of the molecules suggests a separation of the polycyclic aromatic core from the dendritic groups. This arrangement is supported by the relatively weak π-shifts observed for the spacer protons mentioned above. For

(3,4,5)12F8G1-BuPy and **(3,4,5)12F8G1-EtNp** there are, however, indications of a *backfolding* of molecules in the column, which is not observed for **(3,4,5)12F8G1-2EOPy** and **(3,4,5)12F8G1-2EONp**.

In the 2D DQ NMR spectra of **(3,4,5)12F8G1-EtNp** in Figure 4d two different cross-peaks can be distinguished between aromatic and aliphatic protons. The cross-peak depicted in light green can be explained by a spatial proximity of the aromatic protons of the dendron and the alkyl chain, analogous to **(3,4,5)12F8G1-2EOPy** and **(3,4,5)12F8G1-2EONp**. The cross-peak marked light blue, however, indicates a proximity between the naphthalene protons and the alkyl chain. Such proximity could arise from a backfolding of some molecules. In the case of **(3,4,5)12F8G1-BuPy** (Figure 4c) only one cross-peak is observed between the aromatic and the alkyl protons. This could either arise from a proximity of the dendritic aromatic protons and the alkyl chains (light green) or the pyrene protons and the alkyl chains (light blue) or a superposition of both. The corresponding cross-peaks on the alkyl side of the 2D DQ spectrum are missing. This is a phenomenon often observed in the tail region of strong aliphatic peaks. It can be attributed to spectral distortions due to a mobility of the alkyl chains on the NMR time-scale.[18,19] Again, this indicates the possibility of a backfolding of some molecules in the column. The properties of the columnar assembly, however, do not seem to be influenced very significantly by such a backfolding of molecules. Also, the backfolding of **(3,4,5)12F8G1-BuPy** and **(3,4,5)12F8G1-EtNp** has no measurable influence on the π-shifts observed for the aromatic protons of the dendron and the OCH_2R groups (Table 4). If it did, the proximity to the polycyclic aromatic core would cause larger π-shifts than in **(3,4,5)12F8G1-2EOPy** and **(3,4,5)12F8G1-2EONp** (not subject to backfolding effects) and not smaller ones (Table 4). Clearly, for **(3,4,5)12F8G1-BuPy** and **(3,4,5)12F8G1-EtNp** there are indications of a backfolding of molecules in the column. However, backfolding is not observed for **(3,4,5)12F8G1-2EOPy** and **(3,4,5)12F8G1-2EONp**. These results show that a longer and more flexible spacer unit, as in **(3,4,5)12F8G1-2EOPy** and **(3,4,5)12F8G1-2EONp** provides a much better spatial separation of the dendritic and polycyclic aromatic moieties of the molecules and prevents backfolding phenomena much more efficiently.

Investigation of molecular dynamics: We also investigated the molecular dynamics of the four dendritic molecules **(3,4,5)12F8G1-2EOPy**, **(3,4,5)12F8G1-2EONp**, **(3,4,5)12F8G1-BuPy** and **(3,4,5)12G1-EtNp** with homonuclear (^1H,^1H) and heteronuclear (^1H,^{13}C) MAS NMR spinning sideband patterns. These sideband patterns are a sensitive measure for individual homonuclear and heteronuclear dipole–dipole couplings (D_{H-H} and D_{C-H}), which are subject to motional averaging effects. The measured dipole–dipole couplings are compared to coupling values of immobile segments such as CH, CH_2, CH_3 or a phenyl ring, which are calculated from known distances between the nuclei. The typical ^1H–^{13}C bond length of CH_n groups is $r_{C-H} = 1.13$ Å, while the typical distance between two neighboring protons on an aromatic ring is 2.74 Å.[20] Thus, an immobile C–H segment is characterized by a dipole–dipole coupling of $D_{C-H}/2\pi = 21.0$ kHz and an immobile aromatic ring by a ^1H dipole–dipole coupling of $D_{H-H}/2\pi = 8.0$ kHz. These couplings are reduced when molecular motions occur on timescales below 10^{-6} s.[17,21] By relating the measured (reduced) dipole–dipole coupling to the immobile case, a dynamic order parameter S can be determined for individual segments, where $S = 1$ represents a perfectly immobile segment and $S = 0$ isotropic motion.

Starting with ^1H,^1H DQ-spinning sideband patterns in the intracolumnar ordered solid phase (Figure 5), similar patterns are observed for the pyrene or naphthalene protons of the four molecules. A coupling of $D_{H-H}/2\pi = 8.0$ kHz is extracted which corresponds to the full dipole–dipole coupling expected for two neighboring protons ($r_{H-H} = 2.47$ Å). This yields an order parameter of $S_{hom} = 1.0$. On the NMR time scale the pyrene or naphthalene rings are therefore perfectly immobile in their stack. The fitted sideband patterns are obtained from numerical four-spin calculations using the Simpson program.[22] To determine the dipole–dipole coupling of two adjacent protons (2) and (3) in a pyrene or naphthalene ring (marked by the large grey arrow in the inset of Figure 5), the couplings to the neighboring protons on either side (1) and (4) also were taken into account. Thus, a four-spin system with dipole–dipole couplings of $D_{H-H}/2\pi = 8.0$ kHz for neighboring protons (H(1)–H(2), H(2)–H(3) and H(3)–H(4)), $D_{H-H}/2\pi = 1.3$ kHz for every next neighbor (H(1)–H(3) and H(2)–H(4)) and $D_{H-H}/2\pi = 0.4$ kHz for H(1)–H(4) is calculated for an excitation time of four rotor periods, $\tau_{exc} = 4\tau_R$ yielding the sideband patterns depicted in grey in Figure 5. These are in very good agreement to the experimental patterns.

Knowing that the polycyclic aromatic rings are immobile in the intracolumnar ordered solid phase, a heteronuclear dipole–dipole coupling of $D_{C-H}/2\pi = 21.0$ kHz is expected for the pyrene and naphthalene CH groups. Indeed, couplings of $D_{C-H}/2\pi = (20.5 \pm 0.5)-(21.4 \pm 0.5)$ kHz are extracted from REPT-HDOR spinning sideband patterns (not shown), corresponding to order parameters of $S_{het} = 0.98$–1.02.

For the aromatic CH group of the dendron, heteronuclear dipole–dipole couplings of $D_{C-H}/2\pi = 19.0$–21.0 kHz are determined for molecules **(3,4,5)12F8G1-2EONp**, **(3,4,5)12F8G1-BuPy** and **(3,4,5)12G1-EtNp** below T_g, as shown in Figure 6. These couplings correspond to order parameters of $S_{het} = 0.90$–1.0. Quite clearly, not only the polycyclic aromatic rings, but also the dendritic units must be rather immobile in the solid phase.

Turning to the LC phase, only homonuclear but no heteronuclear spinning sideband patterns could be recorded due to the poor ^{13}C signal intensity. From the DQ spinning sideband patterns in Figure 7, recorded at ~60 °C, it can be seen, that the pyrene and naphthalene rings are not immobile any more in the stack. For **(3,4,5)12F8G1-BuPy** a residual ^1H dipole–dipole coupling of $D_{H-H}/2\pi = 5.1$ kHz is extracted. This corresponds to a dynamic order parameter of S_{hom}

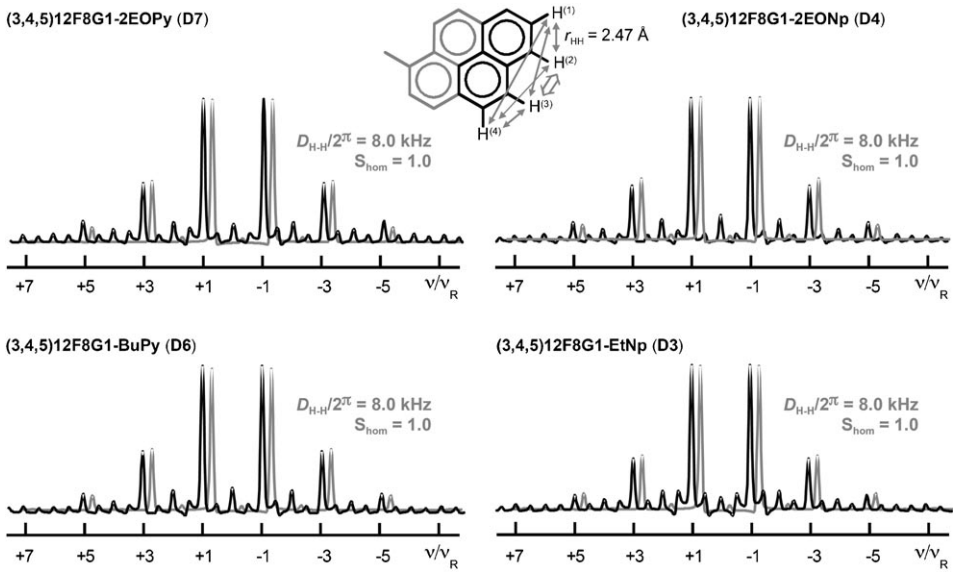

Figure 5. ^{1}H,^{1}H DQ spinning sideband patterns of the polycyclic aromatic core (pyrene/naphthalene) of **(3,4,5)12F8G1-2EOPy**, **(3,4,5)12F8G1-2EONp**, **(3,4,5)12F8G1-BuPy** and **(3,4,5)12G1-EtNp** in the intracolumnar ordered solid phase at 10 °C, recorded under MAS at 30 kHz and an excitation time of four rotor periods ($\tau_{exc}=4\tau_R$). The black and grey lines represent experimental and calculated data, respectively. The insert depicts schematically the dipole–dipole couplings between four ^{1}H spins in a pyrene or naphthalene ring.

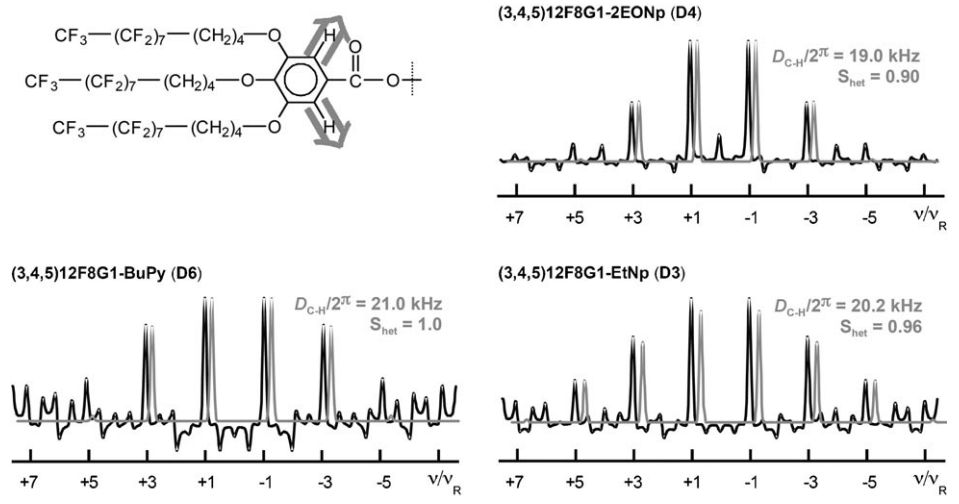

Figure 6. ^{1}H,^{13}C REPT-HDOR spinning sideband patterns of the aromatic CH groups of **(3,4,5)12F8G1-2EONp**, **(3,4,5)12F8G1-BuPy** and **(3,4,5)12G1-EtNp** in the intracolumnar ordered solid phase at 10 °C, recorded under MAS at 30 kHz and a recoupling time of two rotor periods ($\tau_{rcpl}=2\tau_R$) for **(3,4,5)12F8G1-2EONp** and **(3,4,5)12F8G1-BuPy** and $\tau_{rcpl}=3\tau_R$ for **(3,4,5)12G1-EtNp**. The black and grey lines represent experimental and calculated data, respectively. The coupling vector is indicated in the insert.

$\approx$0.65, showing that the pyrene rings of **(3,4,5)12F8G1-BuPy** display some mobility in the π-stack. A fast axial rotation of the molecules in the stack can be excluded, because it would yield an order parameter of $S_{hom}=0.5$, as discussed in reference [3b]. Moreover, the dendritic moieties of the molecules are expected to stabilize the columnar packing significantly, which makes a rotation around the axis of the column highly unlikely anyway. Thus, the most probable motion of the polycyclic aromatic rings in the central stacks is a small angle motion of approximately $\pm 20°$.[23] Figure 7 demonstrates clearly that the aromatic cores of **(3,4,5)12F8G1-2EOPy** and **(3,4,5)12G1-2EONp** are a lot more mobile in the liquid crystalline phase than **(3,4,5)12F8G1-BuPy**, which can be attributed to the different spacer. The residual ^{1}H,^{1}H dipole–dipole coupling extracted from the sidebands of **(3,4,5)12F8G1-2EOPy** and **(3,4,5)12G1-2EONp** is $D_{H-H}/2\pi < 0.6$ kHz and results in an order parameter of $S_{hom} < 0.08$. Recalling the spectra in Figure 3 the higher mobility of molecules **(3,4,5)12F8G1-2EOPy** and **(3,4,5)12G1-2EONp** in the LC phase, as compared to **(3,4,5)12F8G1-BuPy**, is already apparent from the much narrower lines. Such a large mobility of the pyrene and naphthalene rings cannot be explained by an axial rotation or some other in-plane motion, but must rather be due to a fairly large out of plane motion of the rings. Since the LC phase is hexagonal columnar, this motion must occur within the stack, without destroying the columnar arrangement. Thus, the stability of the columns must be attributed to the dendritic units, while the π-interactions between pyrene and naphthalene molecules in the center of the column only play a minor role. In this way, a rather large out of plane motion of the pyrene and naphthalene rings can be explained, which does not affect the overall columnar structure because it is determined by the dendritic units. Such a defined packing of the dendritic units in the column certainly restricts the motions possible for the polycyclic aromatic rings in the core of the column, where a shorter and more rigid spacer as in **(3,4,5)12F8G1-BuPy** will restrict the motion of the pyrene and naphthalene rings to a larger extent than a longer more flexible spacer as in **(3,4,5)12F8G1-2EOPy** and **(3,4,5)12G1-2EONp**. In this way, the different type of spacers can account for the significantly different dynamical

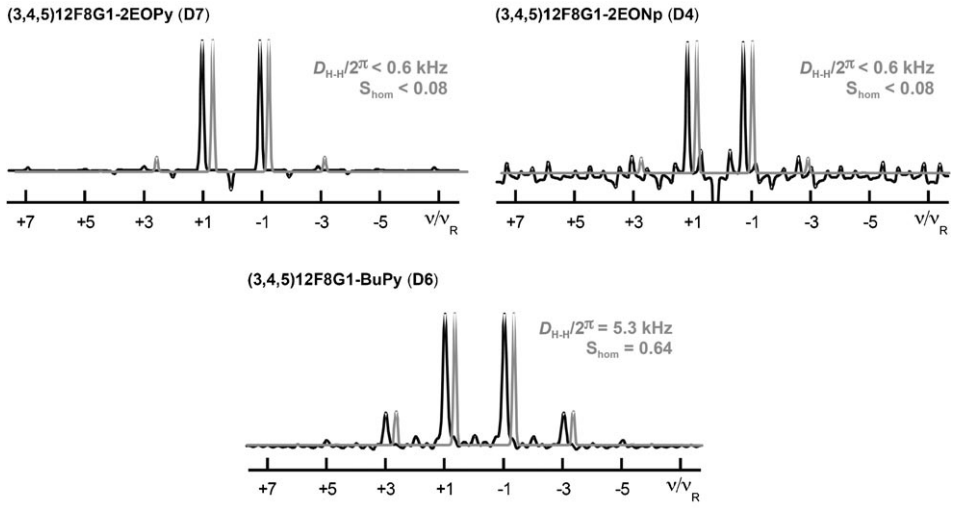

Figure 7. $^{1}H,^{1}H$ DQ spinning sideband patterns of the polycyclic aromatic core (pyrene/naphthalene) of **(3,4,5)12F8G1-2EOPy**, **(3,4,5)12F8G1-2EONp**, **(3,4,5)12F8G1-BuPy** in the LC phase at ~60 °C. The sideband patterns of **(3,4,5)12F8G1-2EOPy** and **(3,4,5)12F8G1-2EONp**, were recorded at 20 kHz MAS with an excitation time of $\tau_{exc}=32\ \tau_R$, while the sideband pattern of **(3,4,5)12F8G1-BuPy** was recorded at 30 kHz MAS and $\tau_{exc}=4\ \tau_R$. The black and grey lines represent experimental and calculated data, respectively. No sideband pattern was recorded for **(3,4,5)12G1-EtNp** since it does not form a stable LC phase.

properties of the pyrene and naphthalene rings in the liquid crystalline phase of **(3,4,5)12F8G1-2EOPy** and **(3,4,5)12G1-2EONp** as compared to **(3,4,5)12F8G1-BuPy**. A detailed understanding of the molecular dynamics of the polycyclic aromatic cores is helpful for designing intracolumnar ordered and stable stable columnar assemblies which exhibit promising charge carrier mobilities.

Molecular model: A simplified molecular model of this self-assembly process is illustrated in Figure 8. For simplicity, the aromatic part of the dendron is shown in red, the electroactive donor in yellow, the alkyl semifluorinated groups in blue and the spacer in black. Also, for simplicity and better visualization in this Figure the dendrons are not tilted. The preassembly process that includes the backfolded structural defects generated from the undesirable packing of the dendron and aromatic donor shown in brown is illustrated on top of the middle column from the left side. Preassembly is followed by the self-assembly of the supramolecular columns that self-organize in the hexagonal columnar lattice containing a mixture of backfolded and correctly arranged stacks of aromatic donors. The backfolded donors are visualized by NMR while the correctly folded units by XRD. The original hexagonal columnar periodic array contains the backfolded structural defects. Heating this hexagonal columnar LC into the isotropic state followed by slow cooling self-repairs these defects and produces the structure shown in the right side of Figure 7. As reported in Table 1, below the Φ_h and $\Phi_{r\text{-}c}$ phases there is a higher order phase which exhibits intracolumnar order. In all cases the higher order phase is also pyramidal hexagonal or rectangular. Preliminary structural analysis by XRD experiments suggest that the higher order phase must mediate even higher charge carrier mobilities than the Φ_h and $\Phi_{r\text{-}c}$ phases reported previously for these compounds.[8b]

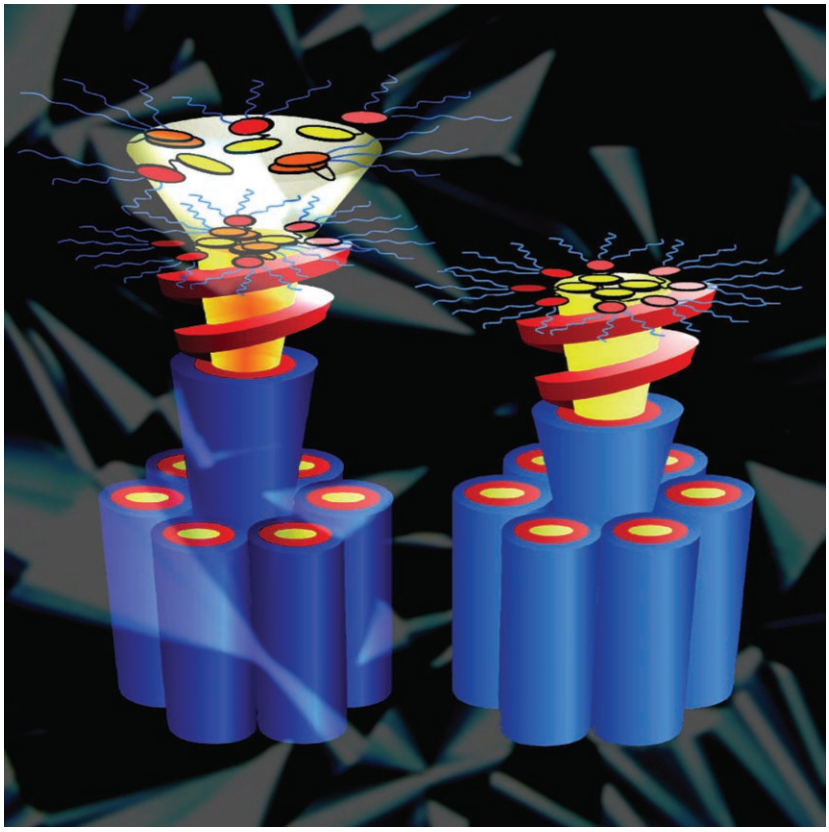

Figure 8. Schematic model of the self-assembly process.

Conclusion

The results reported herein have demonstrated that the attachment of electron-donor groups to a semifluorinated first-generation dendron or minidendron mediates the self-assembly of the donor groups in a π-stack located in the centre of supramolecular helical pyramidal columns. The helical supramolecular columns self-organize into various columnar liquid crystal phases able to enhance the charge carrier mobility of the donor groups from that of the corresponding molecules in amorphous state.[8b] The use of various electron-donors, spacers and first-generation semifluorinated dendrons has shown that this concept is general. The results reported here are expected to impact the field of supramolecular electronics. In addition they demonstrate that the pyramidal liquid crystal phase is, most probably, more general than previously considered.[27] It also demonstrates the utility of the fluorophobic effect or fluorous phase[8b,9b,10,28] in the self-assembly of new classes of pyramidal liquid crystals.[29] Structural analysis data suggest that the higher order phases particularly those exhibiting a higher intracolumnar order[30] than the conventional columnar LC phases are expected to display even higher charge carrier mobilities than those reported previously for the same donor groups in columnar LC phases.[8b] Both the helicity and the intracolumnar order of these supramolecular columns resemble those encountered in supramolecular porous assemblies.[30] The helical pyramidal columnar assemblies exhibiting intracolumnar order play a major role in the structural origin of functions.[8b,30] Research on the elucidation of the principles via which helical supramolecular columns with intracolumnar order are generated is in progress.

Experimental Section

Materials: 3,5-Dimethoxyphenol (**1**; 98%), 1-ethoxynaphthalene (**13**; 97%), methyl 3,4,5-trihydroxybenzoate (**17**; 98%), DCC (99%), 2,3-dihydropyran (97%), α,α,α-trifluorotoluene (99%), *p*-toluene sulfonic acid (PTSA) (98%), tricaprylylmethylammonium chloride (Aliquat 336), $LiAlH_4$ (95%), 1,1,2-trichloro-1,2,2-trifluoroethane (Freon 113), diethylene glycol (98%), 2-(2-chloroethoxy)ethanol (**2**; 99%), pyrrolidine, BH_3 (1 M solution in THF), (all from Aldrich), perfluorooctyl iodide (>98%, Fluka), 1,8-octadiene (**14**), triphenylphosphine, hydrobromic acid (48%), benzyl bromide, tosyl chloride, sodium hydride (60% in mineral oil), 3,5-dimethoxyphenol (97%), K_2CO_3, KOH, MeOH, EtOH, HCl (Fischer), 10% Pd/C and $PdCl_2$ (97%, Lancaster) were used as received. DMF (ACS reagent, Fisher Scientific) was dried over CaH_2 and distilled under vacuum. Et_2O, Bu_2O and THF (ACS reagent, Fisher Scientific) were dried over sodium/benzophenone nd distilled. Et_3N was dried over CaH_2. CH_2Cl_2 was distilled from CaH_2. Hexanes (ACS reagent, Fisher Scientific) used for the Pd^0-catalyzed coupling of perfluorooctyl iodide was washed three times with concentrated H_2SO_4, three times with H_2O, 10% Na_2CO_3 and with H_2O and dried over anhydrous $MgSO_4$ and finally distilled over sodium before use. Carbazole (**10**, 98%, Fluka) was recrystallized twice from THF. Phenothiazine (**6**, 98%, Aldrich) was dissolved in Et_2O to filter off green oxidation products before recrystallization from EtOH and subsequent sublimation. 3,4,5-Tris-(12,12,12,11,11,10,10,9,9,8,8,7,7,6,6,5,5-heptadecafluoro-*n*-dodecyloxy)benzoic acid (**12**),[10a] 1-bromo-12,12,12,11,11,10,10,9,9,8,8,7,7,6,6,5,5-heptadecafluoro-*n*-dodecane (**2**),[10a] 2-[2-(2-chloroethoxy)ethoxy]tetrahydropyran (**7**),[24] 2-[2-(carbazol-9-yl)ethoxy]ethanol (**19**),[15] 4-(dimethylamino)pyridinium *p*-toluenesulfonate (DPTS),[25] 2-{2-[2-(2-benzylethoxy)ethoxy]ethoxy}-*p*-toluene sulfonate (**9**)[13] and 3,5-(dipyrrolidine-1-yl)phenol (**4**)[11] were synthesized according to literature procedures. The synthesis of {2-[2-(carbazol-9-yl)ethoxy]ethyl}3,4,5-tris-(12,12,12,11,11,10,10,9,9,8,8,7,7,6,6,5,5-heptadecafluoro-*n*-dodecan-1-yloxy)benzoate **(3,4,5)12F8G1-2EOCz** (**D8**), {2-[2-((1-naphthyl)acetoxy)ethoxy]ethyl}3,4,5-tris(12,12,12,11,11,10,10,9,9,8,8,7-,7,6,6,5,5-heptadecafluoro-*n*-dodecan-1-yloxy)benzoate **(3,4,5)12F8G1-2EONp** (**D4**), {2-[2-((1-pyrenyl)acetoxy)ethoxy]ethyl}3,4,5-tris-(12,12,12,11,11,10,10,9,9,8,8,7,7,6,6,5,5-heptadecafluoro-*n*-dodecan-1-yloxy)benzoate **(3,4,5)12F8G1-2EOPy** (**D7**) and [4-(1-pyrenyl)-butyl] 3,4,5-tris-(12,12,12,11,11,10,10,9,9,8,8,7,7,6,6,5,5-hepta-decafluoro-*n*-dodecan-1-yloxy)benzoate **(3,4,5)12F8G1-BuPy** (**D6**) has been described previously.[8b] All other conventional materials and solvents were commercially available and were used without further purification.

Techniques: ^1H (500 MHz) and ^{13}C (125 MHz) NMR spectra in solution were recorded on a Bruker DRX-500. Chromatographic purifications were conducted using 200–400 mesh silica gel obtained from Natland International Corporation, Morrisville, NC. The solid-state ^1H NMR experiments were performed on a Bruker DRX spectrometer at a ^1H Larmor frequency of 700 MHz (corresponding to a static magnetic field of 16.4 Tesla). Fast magic-angle spinning (MAS) was applied at a frequency of 30 kHz, using MAS rotors with 2.5 mm outer diameter. The sample temperature was varied between 30 and 110 °C and calibrated, under these fast MAS conditions, following the procedure given in reference [26]. Thin-layer chromatography (TLC) was performed on precoated TLC plates (silica gel with F_{254} indicator; layer thickness, 200 mm; particle size, 5–25 mm; pore size, 60 Å, Sigma-Aldrich). Melting points were measured using a uni-melt capillary melting point apparatus (Arthur H. Thomas Company, Philadelphia, USA) and are uncorrected. High pressure liquid chromatography (HPLC) experiments were performed with a Perkin-Elmer Series 10 GPC equipped with a LC-100 column oven (40 °C), Nelson Analytical 900 Series integrator data station, and two Polymer Laboratories PL gel columns of 5×10^2 and 10^4 Å, and THF as eluent at 1 mL min^{-1}. Detection was by UV absorbance at 254 nm. Thermal transitions were measured on a TA Instruments 2920 modulated differential scanning calorimeter (DSC). In all cases the heating and cooling rates were 10 °C min^{-1}. First order transitions were reported as the maxima or minima of the endothermic and exothermic peaks during the second heating and cooling scans. X-ray diffraction experiments were performed with $Cu_{K\alpha1}$ radiation from a rotating anode (Nonius FR591) X-ray generator and a multi-wire area detector (Siemens). The Cu radiation was collimated and focused with a mirror-monochromator optics. The X-ray beam path is maintained in low vacuum to reduce the background scattering from air. Un-oriented powder samples were kept in a temperature-controlled (± 0.1 °C) oven. Oriented fibers were obtained by extruding the material in the liquid crystalline phase with a mini extruder with a hole diameter of 0.5 or 0.7 mm. Density measurements were carried out by flotation experiments in gradient columns at 20 °C.[9a,d,f] An Olympus BX-40 optical polarized microscope (100× magnification) equipped with a Mettler FP 82 hot stage and a Mettler FP 80 central processor was used to verify thermal transitions and to characterize the anisotropic textures. MALDI-TOF mass spectra were recorded on a PerSpective Biosystems Voyager DE using 2-(4-hydroxyphenylazo)benzoic acid as matrix. Angiotensin I and des-Arg1-Bradykinin were used as standards. Sample preparation was as follows. The matrix (10 mg) was dissolved in 1 mL of THF. The sample (10 mg) was also dissolved in 1 mL of THF. The matrix solution (50 μL) and the sample solution (10 μL) were mixed. To the mixture, 10 mL of the THF solution of AgTFA (1 mg mL^{-1}) was added. The mixture (5 μL) was loaded on a MALDI plate, and air dried before inserting into the vacuum chamber of the MALDI instrument. High resolution mass spectra were run by direct sample introduction on a LCMS (Micromass) platform (electron spray ionizer, electron energy 70 eV). The elemental analysis (C, H) were performed by M-H-W Laboratories, Phoenix, AZ, USA.

2-[2-(3,5-Dimethoxyphenyl)ethoxy]ethanol (3): 3,5-Dimethoxyphenol (**1**; 2.5 g, 0.016 mol), K_2CO_3 (6 g), KI (0.1 g) and 2-(2-chloroethoxy)ethanol (**2;** 1.77 g, 0.016 mol) were added to a round bottom flask containing DMF (50 mL). The mixture was heated at 80 °C for 16 h. The mixture

was poured into H_2O (100 mL) and extracted with Et_2O (3×50 mL). The Et_2O layer was washed with 10% HCl (1×100 mL), dried with $MgSO_4$ and concentrated. The crude material was passed through short silica gel column, using Et_2O as eluent. Evaporation of the solvent gave the title compound as brown oil (2.2 g, 56.8%). Purity (HPLC): 99+%; R_f=0.38 (silica gel; Et_2O); ^{1}H NMR ($CDCl_3$, 500 MHz, 20°C): δ = 6.1 (s, 3H; Ar*H*), 4.1 (t, ^3J(H,H)=4.7 Hz, 2H; ArOCH_2CH$_2$), 3.84 (m, 2H; CH_2), 3.75 (m, 8H; overlap OCH_3 and CH_2), 3.66 (t, ^3J(H,H)=4.7 Hz, 2H; CH_2), 2.35 (brs, 1H; O*H*); ^{13}C NMR ($CDCl_3$, 125 MHz, 20°C): δ = 161.9, 160.9, 94.7, 94.0, 93.8, 73.0, 70.0, 67.8, 67.5, 62.1, 55.7, 55.6; MS: *m*/*z*: calcd for $C_{12}H_{18}O_5$: 242.2719; found: 265.1048 [*M*+Na$^+$].

2-{2-[3,5-(Dipyrrolidin-1-yl)phenyl]ethoxy}ethanol (5): Compound **4** (1.26 g, 0.01 mol), K_2CO_3 (5 g), KI (0.1 g) and 2-(2-chloroethoxy)ethanol (**2**; 1.3 g, 10.5 mmol) were added to a round bottom flask containing of DMF (40 mL). The reaction mixture was heated at 80°C for 24 h. The progress of the reaction was monitored by TLC, which showed complete reaction. The reaction mixture was poured into H_2O (100 mL) and extracted with Et_2O (3×50 mL). The Et_2O layer was washed with 10% HCl, dried with $MgSO_4$ and concentrated. The crude material was passed through short column of silica gel using Et_2O as eluent. The fractions containing the product were collected and the solvent was evaporated to produce the title compound (0.8 g, 25.0%) as a brown oil which solidify upon standing. Purity (HPLC): 99+%; m.p. 71°C; R_f=0.41 (silica gel; Et_2O); ^{1}H NMR ($CDCl_3$, 500 MHz, 20°C): δ = 5.58 (s, 2H; Ar*H ortho* to OCH$_2$CH$_2$), 5.40 (s, 1H; *ortho* to NR$_2$), 4.15 (t, ^3J(H,H)=4.7 Hz, 2H; ArOCH_2CH$_2$), 3.85 (t, ^3J(H,H)=4.7 Hz, 2H; CH_2), 3.72 (m, 2H; CH_2), 3.67 (m, 2H; CH_2), 3.26 (m, 8H; 4CH_2N), 2.23 (m, 1H; O*H*), 1.95 (m, 8H; 4CH_2CH$_2$N); ^{13}C NMR ($CDCl_3$, 125 MHz, 20°C): δ = 161.1, 150.3, 89.6, 88.0, 72.9, 70.4, 67.6, 62.3, 48.2, 25.9; MS: *m*/*z*: calcd for $C_{18}H_{28}N_2O_3$: 320.4319; found: 321.219 [*M*+H$^+$].

2-(2-Phenothiazine-10-yl-ethoxy)ethanol (8): Compound **8** was prepared using a modified literature procedure.[12] Phenothiazine **6** (3.8 g, 19 mmol) and NaH (1.5 g, 37.5 mmol; 60% suspension in mineral oil) were added to of dry, freshly distilled dibutyl ether (30 mL). The mixture was heated at 135°C for 60 min under N_2. 2-[2-(2-Chloroethoxy)ethoxy]-tetrahydropyran (**7**)[24] (8.0 g, 38 mmol) and NaI (0.1 g) were added and the reaction mixture was stirred for 48 h under N_2. The reaction mixture was poured into H_2O (100 mL). A precipitate formed upon cooling at 0°C, which was filtered, washed with water and dried. The crude product was used on the next step without further purification. To a solution of the crude product obtained from the previous step in MeOH (150 mL) was added 10 mL of 10% HCl. The reaction mixture was heated under reflux for 45 min. The mixture was poured into water (20 mL) and neutralized with K_2CO_3. The product was extracted with Et_2O and the organic phase was washed with H_2O, dried with $MgSO_4$ and evaporated. The residue was further purified by column chromatography (silica gel, EtOAc/hexanes 1:1) to yield the title compound as a viscous oil (2.9 g, 53%). Purity (HPLC): 99+%; R_f=0.57 (silica gel; EtOAc/hexanes 60:40); ^{1}H NMR ($CDCl_3$, 500 MHz, 20°C): δ = 7.1 (m, 4H; Ar*H*), 6.9 (m, 4H; Ar*H*), 4.1 (t, ^3J(H,H)=4.7 Hz, 2H; NCH_2), 3.8 (t, ^3J(H,H)= 4.7 Hz, 2H; CH_2), 3.7 (t, ^3J(H,H)=4.7 Hz, 2H; CH_2), 3.6 (t, ^3J(H,H)= 4.7 Hz, 2H; CH_2), 2.0 (brs, 1H; OH); ^{13}C NMR ($CDCl_3$, 125 MHz, 20°C): δ = 145.5, 128.0, 127.7, 125.6, 123.2, 115.9, 72.7, 68.4, 62.2, 47.9; MS: *m*/*z*: calcd for $C_{16}H_{17}NO_2S$: 287.3825 ; found: 310.0868 [*M*$^+$]. The NMR data was consistent with the literature.[12]

2-{2-[2-(2-Carbazol-9-yl-ethoxy)ethoxy]ethoxy}ethanol (11): Carbazole **10** (0.41 g, 2.44 mmol) was added to a suspension of NaH (1 g, 60% in mineral oil) in dry DMF (20 mL). 2-{2-[2-(2-Benzylethoxy)ethoxy]ethoxy}-ethyl *p*-toluene-sulfonate (**9**) (1.0 g, 2.44 mmol) was added and the mixture was stirred at 50°C for 3 h under N_2, after which TLC indicated complete reaction. The mixture was poured (carefully) to water (30 mL). The resulting precipitate was filtered off, dried and used in the next step without further purification. To a solution of the crude product obtained from the previous reaction in EtOH (40 mL) was added Pd/C (0.5 g) catalyst and the mixture was stirred in a hydrogen atmosphere for 24 h at room temperature. The solution was filtered through Celite. Evaporation of the solvent yielded **11** of as a viscous oil (0.2 g, 24%). Purity (HPLC): 99+%; R_f=0.3 (EtOAc/hexanes 6:4); ^{1}H NMR ($CDCl_3$, 500 MHz, 20°C): δ = 8.08 (m, 2H; Ar*H*), 7.46 (m, 4H; Ar*H*), 7.23 (m, 2H; ArH), 4.51 (t, ^3J(H,H)=4.7 Hz, 2H; OCH_2), 3.87 (t, ^3J(H,H)=4.7 Hz, 2H; CH_2), 3.66 (t, ^3J(H,H)=4.7 Hz, 2H; CH_2), 3.53 (m, 10H; overlap 5CH_2), 2.2 (brs, 1H, *OH*); ^{13}C NMR ($CDCl_3$, 125 MHz, 20°C): δ = 141.0, 126.0, 123.3, 120.6, 119.4, 109.3, 72.8, 71.4, 71.0, 70.9, 70.7, 69.7, 62.1, 43.5; CI-MS: cacldc for $C_{20}H_{25}NO_4$: 343.4228 ; found: 344.1875 [*M*+H$^+$].

3,5-Dimethoxyphenyl-3,4,5-tris(12,12,12,11,11,10,10,9,9,8,8,7,7,6,6,5,5-heptadecafluoro-*n*-dodecan-1-yloxy)benzoate [(3,4,5)12F8G1-2EODMB] (D1): A mixture of **12** (0.4 g, 0.25 mmol), **3** (60 mg, 0.25 mmol), DCC (160 mg) and DPTS (0.1 mg) was dissolved in α,α,α-trifluorotoluene (6 mL) and stirred under N_2 at 55°C for 16 h. After cooling down to 25°C, the salts were filtered and the solution precipitated into MeOH. TLC indicated complete conversion. The crude product was precipitated for five times from CH_2Cl_2 into MeOH, then dried in the vacuum oven at 25°C for 24 h to yield the title compound (0.32 g, 70.5%). Purity (HPLC): 99+%; R_f=0.48 (silica gel; EtOAc/hexanes 30:70); ^{1}H NMR ($CDCl_3$, 500 MHz, 20°C): δ = 7.1 (s, 2H; Ar*H*), 6.1 (s, 3H; Ar*H*), 4.5 (t, ^3J(H,H)=4.70 Hz, 2H; CH_2), 4.1 (t, ^3J(H,H)=4.70 Hz, 2H; CH_2), 4.0 (m, 6H; overlapped 3CH_2), 3.9 (t, ^3J(H,H)=5.97 Hz, 4H; 2CH_2), 3.7 (s, 6H; 2OCH_3), 2.2–2.1 (m, 6H; 3CH_2), 1.8 (m, 12H; overlapped 6CH_2); ^{13}C NMR ($CDCl_3$, 125 MHz, 20°C): δ = 166.5, 161.9, 160.9, 152.9, 142.4, 125.6, 120.5–108.2 (several CF multiplets), 108.6, 94.0, 93.5, 73.0, 70.0, 69.8, 68.8, 67.9, 64.5, 55.7, 31.9 (t, J_{CF}=22 Hz), 30.1, 29.1, 17.7, 17.4; MALDI-TOF: *m*/*z*: calcd for $C_{55}H_{43}F_{51}O_9$: 1816.8596; found: 1839.6 [*M*+Na$^+$]; elemental analysis calcd (%) for $C_{55}H_{43}F_{51}O_9$: C 36.36, H 2.39; found: C 36.30, H 2.33.

3,5-(Dipyrrolidin-1-yl)phenyl-3,4,5-tris(12,12,12,11,11,10,10,9,9,8,8,7,7,6,6,5,5-heptadecafluoro-*n*-dodecan-1-yloxy)benzoate [(3,4,5)12F8G1-2EODPB] (D2): A mixture of **12** (0.40 g, 0.25 mmol), **5** (100 mg, 0.25 mmol), DCC (160 mg) and DPTS (0.10 mg) was dissolved in α,α,α-trifluorotoluene (6 mL) and stirred under N_2 at 55°C for 16 h. After cooling down to 25°C, the salts were filtered and the solution precipitated into MeOH. TLC indicated complete conversion. The crude product was precipitated for five times from CH_2Cl_2 into MeOH, then dried in the vacuum oven at 25°C for 24 h to yield the title compound (0.40 g, 84%). Purity (HPLC): 99+%; R_f=0.70 (silica gel; EtOAc/hexanes 30:70); ^{1}H NMR ($CDCl_3$, 500 MHz, 20°C): δ = 7.2 (s, 2H; Ar*H*), 5.6 (s, 2H; Ar*H*), 5.4 (s, 1H; Ar*H*), 4.5 (t, ^3J(H,H)=5.97 Hz, 2H; CH_2), 4.1 (t, ^3J-(H,H)=4.70 Hz, 2H; CH_2), 4.0 (m, 6H; overlapped 3CH_2), 3.9 (t, ^3J-(H,H)=4.70 Hz, 4H; 2CH_2), 3.2 (m, 8H; overlapped 4CH_2), 2.2–2.1 (m, 6H; overlapped 3CH_2), 1.9 (m, 8H; overlapped 4CH_2), 1.8 (m, 12H; overlapped 6CH_2); ^{13}C NMR ($CDCl_3$, 125 MHz, 20°C): δ = 166.5, 161.9, 160.9, 152.9, 142.4, 125.6, 120.5–108.2 (several CF multiplets), 108.6, 94.0, 93.5, 73.0, 70.0, 69.8, 68.8, 67.9, 64.5, 55.7, 31.9 (t, J_{CF}=22 Hz), 30.1, 29.1, 17.7, 17.4; MALDI-TOF: *m*/*z*: calcd for $C_{61}H_{33}F_{51}N_2O_7$: 1895.019; found: 1895.1 [*M*+H$^+$]; elemental analysis calcd (%) for $C_{62}H_{57}F_{51}N_2O_7$: C 38.97, H 3.01; found: C 38.91, H 3.09.

1-Naphthylethyl-3,4,5-tris(12,12,12,11,11,10,10,9,9,8,8,7,7,6,6,5,5-heptadecafluoro-*n*-dodecan-1-yloxy)benzoate [(3,4,5)12F8G1-EtNp] (D3): DCC (300 mg, 1.5 mmol) was added under N_2 to a solution of **12** (1 g, 0.63 mmol), **13** (0.13 g, 0.75 mmol), and DPTS (50 mg, 0.17 mmol) in α,α,α-trifluorotoluene (15 mL), and the reaction mixture was stirred at 45°C for 24 h. The mixture was diluted with CH_2Cl_2 and precipitated in MeOH four times. The crude product was purified by flash column chromatography (silica gel, CH_2Cl_2) and precipitated in EtOH from CH_2Cl_2 solution to yield the title compound as white solid (0.82 g, 75%). Purity (HPLC): 99+%; R_f=0.74 (silica gel; EtOAc/hexanes 30:70); ^{1}H NMR ($CDCl_3$, 500 MHz, 20°C): δ = 8.18 (d, ^3J(H,H)=6.8 Hz, 1H; ArH), 7.88 (d, ^3J(H,H)=6.8 Hz, 1H; ArH), 7.80 (m, 1H, ArH), 7.56–7.50 (m, 2H; ArH), 7.43 (m, 2H; ArH), 7.19 (s, 2H; ArH), 4.67 (t, ^3J(H,H)=5.97 Hz, 2H; CH_2), 4.01 (m, 6H; overlapped 3CH_2), 3.69 (m, 4H; 2CH$_2$), 3.54 (t, ^3J(H,H)=4.4 Hz, 2H, CH_2), 2.18–2.13 (m, 6H; 3CH_2), 1.9–1.8 (m, 12H, 6CH_2); ^{13}C NMR ($CDCl_3$, 90 MHz, 20°C): δ=166.2, 152.4, 141.6, 133.9, 133.8, 132.1, 128.9, 127.5, 127.1, 126.2, 125.7, 125.3, 123.7, 120.5–108.2 (several CF multiplets), 107.8, 72.6, 68.3, 65.2, 30.8 (t, J_{CF}=22 Hz), 29.9, 28.9, 17.5, 17.3; MALDI-TOF: *m*/*z*: calcd for $C_{55}H_{37}F_{51}O_5$: 1746.8143 ; found: 1770.8 [*M*+Na$^+$]; elemental analysis calcd (%) for $C_{55}H_{37}F_{51}O_5$: C 37.82, H 2.13; found: C 37.77, H 2.21.

{2-[2-(Phenothiazine-10-yl)ethoxy]ethyl}-3,4,5-tris(12,12,12,11,,11,10,10,9,9,8,8,7,7,6,6,5,5-heptadecafluoro-*n*-dodecan-1-yloxy)benzoate [(3,4,5)12F8G1-2EOPt] (D5): A mixture containing **12** (1.0 g, 0.63 mmol) and **8** (0.18 g, 0.63 mmol) was dissolved in α,α,α-trifluorotoluene (10 mL) under N_2. DCC (0.388 g, 1.88 mmol) and DPTS (9 mg, 0.03 mmol) were added and the reaction mixture was stirred at 55 °C for 72 h under N_2. The progress of the reaction was monitored by TLC. The organic solution was concentrated and precipitated in MeOH. The crude product was purified by silica gel column chromatography using CH_2Cl_2/EtOAc 3:1 to yield the title compound as white crystals (0.66 g, 57 %). Purity (HPLC): 99+ %; R_f = 0.45 (silica gel; EtOAc/hexanes 30:70); ^{1}H NMR ($CDCl_3$, 500 MHz, 20 °C): δ = 7.1 (m, 4H; Ar*H*), 6.9 (m, 4H; Ar*H*), 4.5 (t, ^3J(H,H) = 5.9 Hz, 4H; 2CH_2), 4.1 (t, ^3J(H,H) = 5.97 Hz, 2H, CH_2), 4.0(m, 6H; 3CH_2), 3.9 (t, ^3J(H,H) = 4.7 Hz, 2H; CH_2), 3.8 (t, ^3J(H,H) = 4.70 Hz, 2H; CH_2), 2.2–2.1 (m, 6H; 3CH_2), 1.8 (m, 12H, overlapped 6CH_2); ^{13}C NMR ($CDCl_3$, 125 MHz, 20 °C): δ = 166.5, 152.9, 145.6, 142.2, 128.1, 127.8, 125.5, 125.2, 123.2, 120.5–108.2 (several CF multiplets), 115.6, 108.9, 73.1, 69.8, 68.8, 64.5, 43.3, 30.6 (t, J_{CF} = 22 Hz), 30.1, 29.1, 17.7, 17.4; MALDI-TOF: *m*/*z*: calcd for $C_{59}H_{42}F_{51}NO_6S$: 1861.9701; found: 1862.7 [*M*+H$^+$], 1885.7 [*M*+Na$^+$], 1901.8 [*M*+K$^+$]; elemental analysis calcd (%) for $C_{59}H_{42}F_{51}NO_6S$: C 38.06, H 2.27; found: C 37.95, H 2.32.

2-{2-[2-(2-Carbazol-9-yl-ethoxy)ethoxy]ethoxy}ethyl-3,4,5-tris-(12,12,12,11,11,10,10,9,9,8,8,7,7,6,6,5,5-heptadecafluoro-*n*-dodecan-1-yloxy)benzoate [(3,4,5)12F8G1-4EOCz] (D10): DCC (300 mg, 1.5 mmol) was added under N_2 to a solution of **12** (0.51 g, 0.64 mmol), **11** (0.1 g, 0.64 mmol), and DPTS (50 mg, 0.17 mmol) in α,α,α-trifluorotoluene (8 mL), and the reaction mixture was stirred at 55 °C for 24 h. The reaction mixture was filtered off to remove insoluble salts. The filtrate solution was concentrate under vacuum and the crude product was precipitated by the addition of methanol (20 mL). The crude product was purified by silica gel column chromatography using CH_2Cl_2/EtOAc 3:1 to yield the title compound as a sticky white solid (0.6 g, 49 %). Purity (HPLC): 99+ %; R_f = 0.36 (silica gel; EtOAc/hexanes 2:3); ^{1}H NMR ($CDCl_3$, 500 MHz, 20 °C): δ = 8.1 (d, ^3J(H,H) = 7.7 Hz, 2H; Ar*H*), 7.4 (m, 4H; Ar*H*), 7.2 (m, 6H; Ar*H*), 4.5 (t, ^3J(H,H) = 5.9 Hz, 4H; ArH), 4.4 (t, ^3J(H,H) = 5.97 Hz, 2H, CH_2), 4.2–4.0 (m, 6H; 3CH_2), 3.86 (t, ^3J(H,H) = 4.70 Hz, 2H; CH_2), 3.7 (t, ^3J(H,H) = 5.97 Hz, 2H; CH_2), 3.54 (m, 2H; CH_2), 3.49 (m, 6H; 3CH_2), 2.3–2.1 (m, 6H; 3CH_2), 1.8 (m, 12H; overlapped 6CH_2); ^{13}C NMR ($CDCl_3$, 125 MHz, 20 °C): δ = 166.5, 152.9, 142.4, 141.0, 126.0, 125.7, 123.3, 120.6, 119.4, 120.5–108.2 (several CF multiplets), 109.3, 108.7, 73.0, 71.4, 71.0, 70.9, 69.7, 69.6, 68.9, 64.6, 43.6, 30.6 (t, J_{CF} = 22 Hz), 30.1, 29.1, 17.7, 17.5; MALDI-TOF: *m*/*z*: calcd for $C_{63}H_{50}F_{51}NO_8$: 1918.0105; found: 1918.6 [*M*+H$^+$], 1941.6 [*M*+Na$^+$], 1957.7 [*M*+K$^+$].

Oct-7-ene-1-ol (15): A 1 M solution of BH_3·THF complex in THF (60 mL, 60 mmol) of was added under N_2 at 0 °C to 1.8-octadiene **14** (22 g, 0.2 mol). The mixture was allowed to reach 25 °C and stirred at this temperature for 1 h, then it was heated under reflux for 1 h. After cooling down to 0 °C, a solution of NaOH (6 gs) in H_2O (30 mL), then 30 % H_2O_2 (20 mL) were subsequently added drop-wise under stirring. The temperature was raised to 25 °C and the mixture was stirred at the same temperature for 12 h. The reaction mixture was poured into Et_2O (150 mL). The ethereal solution was washed with H_2O (2 × 100 mL). The organic phase was dried over $MgSO_4$ and the solvent was distilled off. The resulting crude product was purified by vacuum distillation (b.p. 95 °C, 10 mbar) to give a colorless oil (7.7 g, 30 %). ^{1}H NMR ($CDCl_3$, 500 MHz, 20 °C): δ = 5.83 (m, 1H; CH_2=CHR), 5.01–4.92 (m, 2H; CH$_2$=C*H*R), 3.63 (m, 2H; CH_2OH), 2.04 (m, 2H; CH$_2$=CHCH_2R), 1.55 (m, 6H; CH_2 C2 and C5 positions), 1.35 (m, 6H; CH_2, C3 and C4 positions). The NMR and other analytical data were consistent with the literature.[1]

1-Bromo-16,16,16,15,15,14,14,13,13,12,12,11,11,10,10,9,9-heptadecafluoro-*n*-hexadecane (16):

To a degassed solution of **15** (5.92 g, 45.8 mmol) and perfluorooctyl iodide (25 g, 45.8 mmol) in hexanes (300 mL) and Et_2O (100 mL) was added [Pd(PPh$_3$)$_4$] (3.5 g). The mixture was purged with N_2 and stirred at 25 °C for 24 h. The catalyst was filtered off and washed with ether. The combined ethereal solutions were concentrated and the residue was redissolved in dry THF (200 mL). This solution was added drop-wise to $LiAlH_4$ (2.7 g, 0.14 mol) in dry THF (400 mL) at 0 °C and stirred for 3 h. ^{1}H NMR indicated complete conversion. The excess of $LiAlH_4$ was quenched by slow addition of a 9:1 mixture of THF and water, followed by 10 % NaOH (10 mL). The precipitate was filtered off, washed with THF and the combined filtrates were concentrated. To the resulting residue were added of 48 % HBr (80 mL) and Aliquat-336 (1.1 g) and the mixture was heated under reflux for 12 h. The reaction was cooled to room temperature and extracted with Et_2O (3 × 100 mL). The combined ethereal solution was washed successively with H_2O (2 × 100 mL), saturated $NaHCO_3$ solution (1 × 100 mL) and brine (1 × 100 mL). The organic phase was dried with $MgSO_4$ and the solvent was distilled off. The crude product was dissolved in Freon-113 and filtered over a short silica column. Evaporation of the solvent produced **7** as a white waxy solid (12.5 g, 44.7 % overall yield). M.p. 33 °C: purity (HPLC): 99+ %; R_f = 0.83 (silica gel; Freon-113); ^{1}H NMR ($CDCl_3$, 500 MHz, 20 °C): δ = 3.41 (t, ^3J(H,H) = 6.81 Hz, 2H; CH_2Br), 2.05 (m, 2H; CH_2CF$_2$), 1.86 (m, 2H; CH_2), 1.59 (m, 2H; CH_2), 1.45–1.33 (m, 8H; overlap of 4CH_2); ^{13}C NMR ($CDCl_3$, 125 MHz, 20 °C): δ = 34.2, 33.1, 31.3 (t, J_{CF} = 22.1 Hz), 29.42, 29.38, 28.9, 28.4, 20.5; elemental analysis calcd (%) for $C_{16}H_{16}BrF_{17}$: C 31.44, H 2.64; found: C 31.44, H 2.64.

Methyl 3,4,5-tris-(16,16,16,15,15,14,14,13,13,12,12,11,11,10,10,9,9-heptadecafluoro-*n*-hexadec-1-yloxy) benzoate [(3,4,5)16F8G1-CO$_2$Me]: In a three-neck round-bottom flask equipped with a condenser, Ar inlet-outlet and a magnetic stirrer, a mixture of K_2CO_3 (9 g, 4 equiv) and DMF (150 mL) was thoroughly bubbled with Ar for 0.5 h to eliminate air. Methyl 3,4,5-trihydroxybenzoate (1.2 g, 6.55 mmol) was added and the mixture was heated to 80 °C. 1-Bromo-16,16,16,15,15,14,14,13,13,12,12,11,11,10,10,9,9-heptadecafluoro-*n*-hexadecane (**16**; 12 g, 19.6 mmol) was added and the mixture was stirred under Ar atmosphere at 80 °C for 12 h. TLC analysis showed complete reaction. The reaction mixture was cooled to room temperature and poured into 100 mL of water. The product was extracted with Et_2O (2 × 100 mL). The combined ethereal solution was washed successively with water, 10 % HCl, saturated $NaHCO_3$ and brine. The ethereal solution was dried over $MgSO_4$. The solvent was fully evaporated and the product was recrystallized fro acetone to produce white crystals (4.8 g, 41 %). M.p. 87 °C; purity (HPLC): 99+ %; R_f = 0.80 (EtOAc/hexanes 3:7); ^{1}H NMR ($CDCl_3$, 500 MHz, 20 °C): δ = 7.29 (s, 2H; ArH), 4.05 (t, ^3J(H,H) = 4.7 Hz, 6H; 3OCH_2), 3.91 (s, 3H; CO$_2$CH_3), 2.08 (m, 6H; 3CH_2), 1.85 (m, 4H; 2CH_2), 1.77 (m, 2H; CH_2), 1.62 (m, 6H; 3CH_2), 1.53 (m, 6H; 3CH_2), 1.40 (m, 18H; 9CH_2); ^{13}C NMR ($CDCl_3$, 125 MHz, 20 °C): δ = 167.0, 153.2, 142.6, 125.7, 120.5–108.2 (several CF multiplets), 108.5, 73.8, 69.5, 52.6, 30.6 (t, J_{CF} = 22 Hz), 30.1, 29.71, 29.66, 29.61, 29.5, 26.4, 20.5; MALDI-TOF: *m*/*z*: calcd for $C_{56}H_{53}F_{51}O_5$: 1774.9524; found: 1796.8 [*M*+Na]$^+$.

3,4,5-Tris-(16,16,16,15,15,14,14,13,13,12,12,11,11,10,10,9,9-heptadecafluoro-*n*-hexadec-1-yloxy)benzoic acid [(3,4,5)16F8G1-CO$_2$H] (18): A 20 % KOH solution (10 mL) was added to a solution of **(3,4,5)16F8G1-CO$_2$Me** obtained on the previous step (3.5 g, 3.14 mmol) in EtOH (60 μL). The mixture was heated under reflux for 4 h. TLC analysis showed complete reaction. The solvent was fully evaporated and the resulting potassium salt was dissolved in of THF/water 3:1 (70 mL). The solution was acidified with 2 M HCl until pH 4. Water (70 mL) was added and the product was filtered, washed with water and methanol respectively and dried. Recrystallization from acetone produced **18** as white crystals (3.1 g; 90 %). Purity (HPLC): 99+ %; R_f = 0.63 (EtOAc/hexanes 3:7); ^{1}H NMR ($CDCl_3$, 500 MHz, 20 °C): δ = 7.32 (s, 2H; ArH), 4.04 (t, ^3J(H,H) = 4.7 Hz, 6H, 3OCH_2), 2.03 (m, 6H; 3CH_2), 1.85 (m, 4H; 2CH_2), 1.79 (m, 2H; CH_2), 1.68 (m, 6H; CH_2), 1.55 (m, 6H; 3CH_2), 1.49 (m, 18H; 9CH_2); ^{13}C NMR ($CDCl_3$, 125 MHz, 20 °C): δ = 171.6, 153.2, 143.6, 124.0, 120.5–108.2 (several CF multiplets), 108.9, 73.8, 69.4, 30.6 (t, J_{CF} = 22 Hz), 30.1, 29.71, 29.66, 29.61, 29.5, 26.4, 20.5; elemental analysis calcd (%) for $C_{56}H_{53}F_{51}O_5$: C 37.89, H 3.01; found: C 37.89, H 3.01.

2-(2-Carbazol-9-yl-ethoxy)ethyl-3,4,5-tris-(16,16,16,15,15,14,14,13,13,12,12,11,11,10,10,9,9-heptadecafluoro-*n*-hexadecan-1-yloxy)benzoate [(3,4,5)16F8G1-2EOCz] (D9): DCC (140 mg, 0.68 mmol) was added under N_2 to a solution of **18** (0.4 g, 0.23 mmol), **19** (0.06 g, 0.23 mmol), and DPTS (10 mg) in α,α,α-trifluorotoluene (6 mL), and the reaction

mixture was stirred at 55 °C for 24 h. The reaction mixture was filtered off to remove insoluble salts. The filtrate solution was concentrate under vacuum and the crude product was precipitated by the addition of methanol (20 mL). The crude product was purified by silica gel column chromatography using CH_2Cl_2/EtOAc 3:1 to yield the title compound as white solid (0.35 g, 77 %). Purity (HPLC): 99+ %; R_f = 0.71 (silica gel; EtOAc/hexanes 30:70); ^{1}H NMR ($CDCl_3$, 500 MHz, 20 °C): δ = 8.1 (d, ^3J(H,H) = 7.7 Hz, 2H; ArH), 7.4 (m, 4H; Ar*H*), 7.2 (m, 6H, Ar*H*), 4.5 (t, ^3J(H,H) = 5.9 Hz, 2H; CH_2), 4.4 (t, ^3J(H,H) = 5.97 Hz, 2H; CH_2), 4.0 (m, 2H; CH_2), 3.9 (m, 6H; 3CH_2), 3.7 (t, ^3J(H,H) = 4.7 Hz, 2H; CH_2), 2.3–2.1 (m, 6H; 3CH_2), 1.8 (m, 6H; 3CH_2), 1.6 (m, 8H; 4CH_2), 1.4 (m, 8H; overlapped 4CH_2), 1.3 (m, 16H, overlapped 8CH_2); ^{13}C NMR ($CDCl_3$, 125 MHz, 20 °C): δ = 166.7, 153.2, 142.8, 141.0, 126.1, 125.1, 123.3, 120.6, 119.5, 120.5–108.2 (several CF multiplets), 109.1, 108.5, 73.8, 69.8, 69.5, 43.7, 32.8, 31.4, 31.3, 31.1, 30.7, 29.8, 26.6, 20.5; elemental analysis calcd (%) for $C_{72}H_{68}F_{51}NO_6$: C 42.98, H 3.41; found: C 42.98, H 3.41.

Acknowledgements

Financial support by the National Science Foundation (DMR-0102459 and DMR-0548559) is gratefully acknowledged.

[1] a) P. G. Schouten, J. M. Warman, M. P. De Haas, M. A. Fox, H.-L. Pan, *Nature* **1991**, *353*, 736; b) D. Adam, F. Closs, T. Frey, D. Funhoff, D. Haarer, H. Ringsdorf, P. Schumacher, K. Siemensmeyer, *Phys. Rev. Lett.* **1993**, *70*, 457; c) D. Adam, D. Haarer, F. Closs, T. Frey, D. Funhoff, K. Siemensmeyer, P. Schuhmacher, H. Ringsdorf, *Ber. Bunsen Ges. Phys. Chem.* **1993**, *97*, 1366; d) D. Adam, P. Schuhmacher, J. Simmerer, L. Häussling, K. Siemensmeyer, K. H. Etzbach, H. Ringsdorf, D. Haarer, *Nature* **1994**, *371*, 141; e) P. G. Schouten, J. M. Warman, M. P. De Haas, C. F. van Nostrum, G. H. Gelinck, R. J. M. Nolte, M. J. Copyn, J. W. Zwikker, M. K. Engel, M. Hanack, H. Y. Cheng, W. T. Ford, *J. Am. Chem. Soc.* **1994**, *116*, 6880; f) N. B. Boden, R. C. Borner, R. J. Bushby, J. Clements, *J. Am. Chem. Soc.* **1994**, *116*, 10807.

[2] a) H. Shirakawa, *Angew. Chem.* **2001**, *113*, 2642; *Angew. Chem. Int. Ed.* **2001**, *40*, 2574; b) A. G. MacDiarmid, *Angew. Chem.* **2001**, *113*, 2649; *Angew. Chem. Int. Ed.* **2001**, *40*, 2581; c) A. J. Heeger, *Angew. Chem.* **2001**, *113*, 2660; *Angew. Chem. Int. Ed.* **2001**, *40*, 2591.

[3] a) A. Fechtenkötter, K. Saalwächter, M. A. Harbison, K. Müllen, H. W. Spiess, *Angew. Chem.* **1999**, *111*, 3224; *Angew. Chem. Int. Ed.* **1999**, *38*, 3039; b) S. P. Brown, I. Schnell, J. D. Brand, K. Müllen, H. W. Spiess, *J. Am. Chem. Soc.* **1999**, *121*, 6712; c) S. Ito, M. Wehmeier, J. D. Brand, C. Kübel, R. Epsch, J. P. Rabe, K. Müllen, *Chem. Eur. J.* **2000**, *6*, 4327; d) A. M. van de Craats, J. M. Warman, *Adv. Mater.* **2001**, *13*, 130; e) W. Pisula, M. Kastler, D. Wasserfallen, T. Pakula, K. Müllen, *J. Am. Chem. Soc.* **2004**, *126*, 8074; f) J. Wu, M. Baumgarten, M. G. Debije, J. M. Warman, K. Müllen, *Angew. Chem.* **2004**, *116*, 5445; *Angew. Chem. Int. Ed.* **2004**, *43*, 5331; g) V. Lemaur, D. A. da Silva Filho, V. Coropceanu, M. Lehmann, Y. Geerts, J. Piris, M. G. Debije, A. M. van de Craats, K. Senthilkumar, L. D. A Siebbeles, J. M. Warman, J.-L. Brédas, J. Cornil, *J. Am. Chem. Soc.* **2004**, *126*, 3271; h) Z. Wang, M. D. Watson, J. Wu, K. Müllen, *Chem. Commun.* **2004**, 336; i) M. G. Debije, J. Piris, M. P. de Haas, J. M. Warman, Z. Tomovic, C. D. Simpson, M. D. Watson, K. Müllen, *J. Am. Chem. Soc.* **2004**, *126*, 4641; j) Z. Tomovic, M. D. Watson, K. Müllen, *Angew. Chem.* **2004**, *116*, 773; *Angew. Chem. Int. Ed.* **2004**, *43*, 755; k) M. Kastler, W. Pisula, D. Wasserfallen, T. Pakula, K. Müllen, *J. Am. Chem. Soc.* **2005**, *127*, 4286.

[4] a) A. Reichert, H. Ringsdorf, P. Schumacher, W. Baumeister, T. Scheybani, in *Comprehensive Supramolecular Chemistry, Vol. 9* (Ed.: J. M. Lehn), Elsevier, Oxford (UK), **1977**, pp. 313; b) N. Boden, B. Movaghar, in *Handbook of Liquid Crystals Vol. 2B* (Eds.: D. Demus, J. Goodby, G. W. Gray, H. W. Spiess, V. Vill), Wiley-VCH, Weinheim, **1998**, pp. 781; c) H. Eichhorn, *J. Porphyrins Phthalocyanines* **2000**, *4*, 88; d) N. Bodden, R. J. Bushby, J. Clements, B. Movaghar, *J. Mater. Chem.* **2001**, *9*, 2081; e) F. Würthner, *Angew. Chem.* **2001**, *113*, 1069; *Angew. Chem. Int. Ed.* **2001**, *40*, 1037; f) R. J. Bushby, O. R. Lozman, *Curr. Opin. Colloid Interface Sci.* **2002**, *7*, 343; g) R. J. Bushby, O. R. Lozman, *Curr. Opin. Solid State Mater. Sci.* **2002**, *6*, 569; h) M. O'Neill, S. M. Kelly, *Adv. Mater.* **2003**, *15*, 1135.

[5] a) K. Kanakarajan, A. W. Czarnik, *J. Org. Chem.* **1986**, *51*, 5241; b) K. Pieterse, P. A. van Hal, R. Kleppinger, J. A. J. M. Vekemans, R. A. J. Janssen, E. W. Meijer, *Chem. Mater.* **2001**, *13*, 2675; c) F. Würthner, C. Thalacker, S. Diele, C. Tschierske, *Chem. Eur. J.* **2001**, *7*, 2245; d) M. Lehmann, G. Kestemont, R. G. Aspe, C. Buess-Herman, M. H. J. Koch, M. G. Debije, J. Piris, M. P. de Hass, J. M. Warman, M. D. Waston, V. Lemaur, J. Cornil, Y. H. Geerts, R. Gearba, D. A. Ivanov, *Chem. Eur. J.* **2005**, *11*, 3349.

[6] a) B. A. Gregg, R. A. Cormier, *J. Am. Chem. Soc.* **2001**, *123*, 7959; b) M. Funahashi, J.-I. Hanna, *Phys. Rev. Lett.* **1997**, *78*, 2184; c) P. Vlachos, B. Mansoor, M. P. Aldred, M. O'Neill, S. M. Kelly, *Chem. Commun.* **2005**, *23*, 2921; d) C. W. Struijk, A. B. Sieval, J. E. J. Dakhorst, M. van Dijk, P. Kimkes, R. B. M. Koehorst, H. Donker, T. J. Schaafsma, S. J. Picken, A. M. van de Craats, J. M. Warman, H. Zuilhof, E. J. R. Sudhölter, *J. Am. Chem. Soc.* **2000**, *122*, 11057.

[7] H. Sirringhaus, P. J. Brown, R. H. Friend, M. M. Nielsen, K. Bechgaard, B. M. W. Langeveld-Voss, A. J. H. Spiering, R. A. J. Janssen, E. W. Meijer, P. Herwig, D. M. de Leeuw, *Nature* **1999**, *401*, 685.

[8] a) E. W. Meijer, A. P. H. J. Schenning, *Nature* **2002**, *419*, 353; b) V. Percec, M. Glodde, T. K. Bera, Y. Miura, I. Shlyanovskaya, K. D. Singer, V. S. K. Balagurusamy, P. A. Heiney, I. Schnell, A. Rapp, H. W. Spiess, S. D. Hudson, H. Duan, *Nature* **2002**, *419*, 384; c) A. P. H. J. Schenning, P. Jonkheijm, F. J. M. Hoeben, J. van Herrikhuyzen, S. C. J. Meskers, E. W. Meijer, L. M. Herz, C. Daniel, C. Silva, R. T. Phillips, R. H. Friend, D. Beljonne, A. Miura, S. De Feyter, M. Zdanowska, H. Uji-i, F. C. De Schryver, Z. Chen, F. Würthner, M. Mas-Torrent, D. den Boer, M. Durkut, P. Hadle, *Synth. Met.* **2004**, *43*, 147; d) F. J. M. Hoeben, P. Jonkheijm, E. W. Meijer, A. P. H. J. Schenning, *Chem. Rev.* **2005**, *105*, 1491; e) J. P. Hill, W. Jin, A. Kosaka, T. Fukushima, H. Ichihara, T. Shimomura, K. Ito, T. Hashizume, N. Ishii, T. Aida, *Science* **2004**, *304*, 1481; f) A. P. J. H. Schenning, E. W. Meijer, *Chem. Commun.* **2005**, 3245; g) H. E. Katz, A. J. Lovinger, J. Johnson, C. Kloc, T. Siegrist, W. Li, Y. Y. Lin, A. Dodabalapur, *Nature* **2000**, *404*, 478; h) B. A. Jones, M. J. Ahrens, M.-H. Yoon, A. Facchetti, T. J. Marks, M. R. Wasielewski, *Angew. Chem.* **2004**, *116*, 6523; *Angew. Chem. Int. Ed.* **2004**, *43*, 6363; i) V. Percec, A. Keller, *Macromolecules* **1990**, *23*, 4347.

[9] a) V. Percec, G. Johansson, J. Heck, G. Ungar, S. V. Batty, *J. Chem. Soc. Perkin Trans. 1* **1993**, 1411; b) V. Percec, G. Johnsson, G. Ungar, J. Zhon, *J. Am. Chem. Soc.* **1996**, *118*, 9855; c) S. D. Hudson, H.-T. Jung, V. Percec, W.-D. Cho, G. Johannsson, G. Ungar, V. S. K. Balagurusamy, *Science* **1997**, *278*, 449; d) V. Percec, W.-D. Cho, G. Ungar, D. J. P. Yeardley, *J. Am. Chem. Soc.* **2001**, *123*, 1302; e) V. Percec, W.-D. Cho, G. Ungar, D. J. P. Yeardley, *Chem. Eur. J.* **2002**, *8*, 2011; f) V. Percec, C. M. Mitchell, W.-D. Cho, S. Uchida, M. Glodde, G. Ungar, X. Zeng, Y. Liu, V. S. K. Balagurusamy, P. A. Heiney, *J. Am. Chem. Soc.* **2004**, *126*, 6078; g) G. Ungar, D. Abramic, V. Percec, J. A. Heck, *Liq. Cryst.* **1996**, *21*, 73.

[10] a) G. Johansson, V. Percec, G. Ungar, J. Zhou, *Macromolecules* **1996**, *29*, 646; b) V. Percec, D. Schlueter, Y. K. Kwon, J. Blackwell, M. Moeller, P. J. Slangen, *Macromolecules* **1995**, *28*, 8807; c) G. Johansson, V. Percec, G. Ungar, K. Smith, *Chem. Mater.* **1997**, *9*, 164; d) D. R. Dukeson, G. Ungar, V. S. K. Balagurusamy, V. Percec, G. A. Johansson, M. Glodde, *J. Am. Chem. Soc.* **2003**, *125*, 15974.

[11] F. Effenberger, R. Niess, *Chem. Ber.* **1968**, *101*, 3787.

[12] K. E. Andersen, J. L. Sorensen, J. Lau, B. F. Lundt, H. Petersen, P. O. Huusfeldt, P. D. Suzdak, M. D. B. Swedberg, *J. Med. Chem.* **2001**, *44*, 2152.

[13] C. Selve, S. Achilefu, L. Mansuy, *Synth. Commun.* **1990**, *20*, 799.

[14] H. Matsuda, A. Yamamoto, N. Iwamoto, S. Matsuda, *J. Org. Chem.* **1978**, *43*, 4567.

[15] C. I. Simionescu, V. Percec, A. Natansohn, *Polym. Bull.* **1981**, *4*, 623; C. I. Simionescu, V. Percec, A. Natansohn, *Polym. Bull.* **1980**, *3*, 535.
[16] a) V. Percec, C-H. Ahn, T. K. Bera, G. Ungar, D. J. P. Yeardley, *Chem. Eur. J.* **1999**, *5*, 1070; b) V. Percec, W. D. Cho, G. Ungar, D. J. P. Yeardley, *J. Am. Chem. Soc.* **2001**, *123*, 1302.
[17] A. Rapp, I. Schnell, D. Sebastiani, S. P. Brown, V. Percec, H. W. Spiess, *J. Am. Chem. Soc.* **2003**, *125*, 13284.
[18] S. P. Brown, I. Schnell, J. D. Brand, K. Müllen, H. W. Spiess, *Phys. Chem. Chem. Phys.* **2000**, *2*, 1735.
[19] I. Schnell, S. P. Brown, H. Y. Low, H. Ishida, H. W. Spiess, *J. Am. Chem. Soc.* **1998**, *120*, 11784.
[20] C. Ochsenfeld, F. Koziol, S. P. Brown, T. Schaller, U. P. Seebach, F. G. Klärner, *Solid State Nucl. Magn. Reson.* **2002**, *22*, 128.
[21] S. P. Brown, H. W. Spiess, *Chem. Rev.* **2001**, *101*, 4125.
[22] M. Bak, J. T. Rasmussen, N. C. Nielsen, *J. Magn. Reson.* **2000**, *147*, 296.
[23] D. Hentschel, H. Sillescu, H. W. Spiess, *Polymer* **1981**, *22*, 1516.
[24] B. Dietrich, W. M. Hosseini, J.-M. Lehn, R. B. Sessions, *Helv. Chim. Acta* **1985**, *68*, 289.
[25] J. S. Moore, S. I. Stupp, *Macromolecules* **1990**, *23*, 65.
[26] B. Langer, I. Schnell, H. W. Spiess, A.-R. Grimmer, *J. Magn. Reson.* **1999**, *138*, 182.
[27] a) H. Zimmermann, R. Poupko, Z. Luz, J. Billard, *Z. Naturforsch. A* **1985**, *40a*, 149; b) J. Malthête, A. Collet, *Nouv. J. Chim.* **1985**, *9*, 15; c) A. M. Levelut, J. Malthête, A. Collet, *J. Phys.* **1986**, *47*, 351; d) J. Malthête, A. Collet, *J. Am. Chem. Soc.* **1987**, *109*, 7544; e) R. Poupko, Z. Luz, N. Spielberg, H. Zimmermann, *J. Am. Chem. Soc.* **1989**, *111*, 6094; f) H. Zimmermann, V. Bader, R. Poupko, E. J. Wachtel, Z. Luz, *J. Am. Chem. Soc.* **2002**, *124*, 15286.
[28] a) C. Rocaboy, F. Hampel, J. A. Gladysz, *J. Org. Chem.* **2002**, *67*, 6863; b) Y. Tang, G. Ghirlanda, N. Vaidehi, J. Kua, D. T. Mainz, W. A. Goddard III, W. F. DeGrado, D. A. Tirrel, *Biochemistry* **2001**, *40*, 2790; c) S. Sheiko, E. Lermann, M. Möller, *Langmuir* **1996**, *12*, 4015; d) *Handbook of Fluorous Chemistry* (Eds.: J. A. Gladysz, D. P. Curran, I. T. Horvath), Wiley-VCH, Weinheim, **2004**.
[29] a) V. Percec, M. Glodde, G. Johansson, V. S. K. Balagurusamy, P. A. Heiney, *Angew. Chem.* **2003**, *115*, 4403; *Angew. Chem. Int. Ed.* **2003**, *42*, 4338; b) V. Percec, M. R. Imam, T. K. Bera, V. S. K. Balagurusamy, M. Peterca, P. A. Heiney, *Angew. Chem.* **2005**, *117*, 4187; *Angew. Chem. Int. Ed.* **2005**, *44*, 4739.
[30] a) V. Percec, A. E. Dulcey, V. S. K. Balagurusamy, Y. Miura, J. Smidrkal, M. Peterca, S. Nummelin, U. Edlund, S. D. Hudson, P. A. Heiney, H. Duan, S. N. Magonov, S. A. Vinogradov, *Nature* **2004**, *430*, 764; b) V. Percec, A. Dulcey, M. Peterca, M. Ilies, Y. Miura, U. Edlund, P. A. Heiney, *Aust. J. Chem.* **2005**, *58*, 472; c) V. Percec, A. E. Dulcey, M. Peterca, M. Ilies, J. Ladislaw, B. M. Rosen, U. Edlund, P. A. Heiney, *Angew. Chem.* **2005**, *117*, 6674; *Angew. Chem. Int. Ed.* **2005**, *44*, 6516; d) V. Percec, J. Rudick, M. Peterca, M. Wagner, M. Obata, C. M. Mitchell, W.-D. Cho, V. S. K. Balagurusamy, P. A. Heiney, *J. Am. Chem. Soc.* **2005**, *127*, 15257; e) V. Percec, A. E. Dulcey, M. Peterca, M. Ilies, M. J. Sienkowska, P. A. Heiney, *J. Am. Chem. Soc.* **2005**, *127*, 17902.

Received: September 28, 2005
Revised: March 3, 2006
Published online: May 23, 2006

